NTS-1308

SAND81-1970 • Unlimited Release • UC-70

Printed April 1983

Petrology and Geochemistry of the Grouse Canyon Member of the Belted Range Tuff, Rock-Mechanics Drift, U12g Tunnel, Nevada Test Site

James R. Connolly, William L. Mansker, Randall Hicks,
Carlton C. Allen, John Husler, Klaus Keil, Allen R. Lappin

Prepared by
Sandia National Laboratories
Albuquerque, New Mexico 87185 and Livermore, California 94550
for the United States Department of Energy
under Contract DE-AC04-76DP00789

Issued by Sandia National Laboratories, operated for the United States Department of Energy by Sandia Corporation.

Printed in the United States of America
Available from
National Technical Information Service
U.S. Department of Commerce
5285 Port Royal Road
Springfield, VA 22161

NTIS price codes
Printed copy: A04
Microfiche copy: A01

SAND81-1970
Unlimited Release
Printed April 1983

Distribution
Category UC-70

Petrology and Geochemistry of the Grouse Canyon Member of the Belted Range Tuff, Rock-Mechanics Drift, U12g Tunnel, Nevada Test Site

James R. Connolly, William L. Mansker,
Randall Hicks, Carlton C. Allen, John Husler,
and Klaus Keil
Department of Geology
Institute of Meteoritics
University of New Mexico
Albuquerque, NM 87131

Allen R. Lappin
NNWSI Geotechnical Projects Division 9763
Sandia National Laboratories
Albuquerque, NM 87185

Abstract

G-Tunnel at Nevada Test Site (NTS) is the site of thermal and thermomechanical experiments examining the feasibility of emplacing heat-producing nuclear wastes in silicic tuffs. This report describes the general stratigraphy, mineralogy, and bulk chemistry of welded portions of the Grouse Canyon Member of the Belted Range Tuff, the unit in which most of these experiments will be performed. The geologic characteristics of the Grouse Canyon Member are compared with those of the Topopah Spring Member of the Paintbrush Tuff, presently the preferred horizon for an actual waste repository at Yucca Mountain, near the southwest boundary of Nevada Test Site. This comparison suggests that test results obtained in welded tuff from G-Tunnel are applicable, with limitations, to evaluation of the Topopah Spring Member at Yucca Mountain.

Acknowledgments

W. C. Vollendorf, Div 7133, B. S. Langkopf, Div 9762, and R. M. Zimmerman, Div 9763, of Sandia National Laboratories provided technical and logistical assistance in sample procurement and analysis. G-Tunnel personnel assisted in sampling in the Rock-Mechanics Drift. P. H. Warren of the University of New Mexico wrote the computer program to calculate bulk molecular norms and assisted in the calculations. B. S. Langkopf and W. C. Vollendorf provided helpful technical reviews of the report.

Contents

Figures

Figures (Cont)

Tables

Acronyms

CHLW	Commercial high-level nuclear waste
DOE	US Department of Energy
NNWSI	Nevada Nuclear Waste Storage Investigation
NTS	Nevada Test Site
RMA	Rock-Mechanics Alcove
RMD	Rock-Mechanics Drift
SEM	Scanning-electron microscopy (or microscope)
XRD	X-ray powder diffraction

Petrology and Geochemistry of the Grouse Canyon Member of the Belted Range Tuff, Rock-Mechanics Drift, U12g Tunnel, Nevada Test Site

Introduction

The petrography, petrology, and geochemistry of any medium considered for storage of commercial high-level nuclear waste (CHLW) are indirectly important parameters in repository design and construction. Thermomechanical and hydrologic properties of the host rock are engineering properties of prime concern; host-rock mineralogy, texture, and fabric are important in understanding variations in these properties. A thorough understanding of the geochemistry of the emplacement medium is critical in understanding its response to chemical changes and thermal excursions imposed by emplacement of CHLW.

This report briefly summarizes the petrology and geochemistry of the Grouse Canyon Member of the Belted Range Tuff[1] as exposed in the Rock-Mechanics Drift (RMD), part of the U12g Tunnel (G-Tunnel) beneath Rainier Mesa on the Nevada Test Site (NTS) (Figure 1). Some additional information is provided for underlying and overlying tuffs. In addition, the report considers potential transferability of data from G-Tunnel to the Topopah Spring Member of the Paintbrush Tuff at Yucca Mountain (NTS), a potential repository horizon.

G-Tunnel *is not* being considered as a repository location; it is the site of a series of medium-specific thermomechanical experiments and heater tests designed to aid in developing experimental and site-characterization techniques and in assessing the feasibility (from a thermal and mechanical viewpoint) of emplacing nuclear wastes in silicic tuffs. The work described here was performed as part of the Nevada Nuclear Waste Storage Investigations (NNWSI) project, administered by the Nevada Operations Office of the US Department of Energy (DOE) in Las Vegas, NV.

The study is based on a suite of 16 samples collected November 7, 1980, from the left rib of the RMD, and on 4 supplemental samples collected March 25, 1981, from Hole U12g-RM-P1 (Figure 2). The samples cover a stratigraphic interval of about 17 m (56 ft), which includes the Grouse Canyon Member of the Belted Range Tuff, plus some of the underlying Tunnel Bed 5 and overlying Upper Transition Zone; both of the latter units are informal. Samples include a representative suite of tuffs, argillaceous material from matrices of rubble flow zones, fault and fracture fillings, and clay "pods" within the matrix of the welded Grouse Canyon Member. The analytical techniques used on various rock types include transmitted- and reflected-light microscopy, whole-rock chemical analyses for major and minor elements, x-ray diffraction of clays and zeolites, electron-microprobe analysis of glass and various phenocrysts and crystallization products, and combined scanning-electron microscopy (SEM) and energy-dispersive x-ray analysis.

Field Aspects of the Grouse Canyon Member in the Rock-Mechanics Drift (RMD)

Structural field characteristics of the welded Grouse Canyon Member are not the main focus of this report. These aspects, especially fracturing, are described in a companion report by Langkopf and Eshom.[2] Sufficient discussion is included here to place individual samples in perspective within the unit as a whole. Most samples collected for analysis are from the left rib of the Rock-Mechanics Drift (RMD) (Figure 2). The RMD was driven on a 15° positive incline on a N35°W bearing, for a distance of about 34 m (112 ft). As shown in Figure 2, the RMD cuts through the

Grouse Canyon Member, providing access both to the top of the unit, for conducting relatively large-scale experiments, and to the middle of the unit, where small-diameter heater tests and a heated-block experiment are to be performed.[3] The apparent dip of the Grouse Canyon Member is about 9° NW on the left rib of the RMD. The Rock-Mechanics Alcove (RMA) was driven southwest, perpendicular to the RMD, about 30 m (100 ft) from the foot of the RMD. Hole U12g-RM-P1, from which supplemental samples were taken, was drilled downward through the Grouse Canyon Member from the RMA, approximately perpendicular to layering. The RMA has since been lengthened to form the Experiment Drift, shown in plan view as part of Figure 3. The apparent thickness of the Grouse Canyon Member is about 14 m (45 ft) in the RMD, measured between the top of Tunnel Bed 5 and the pale reddish-brown horizon that marks the base of the Upper Transition Zone overlying the Grouse Canyon Member.

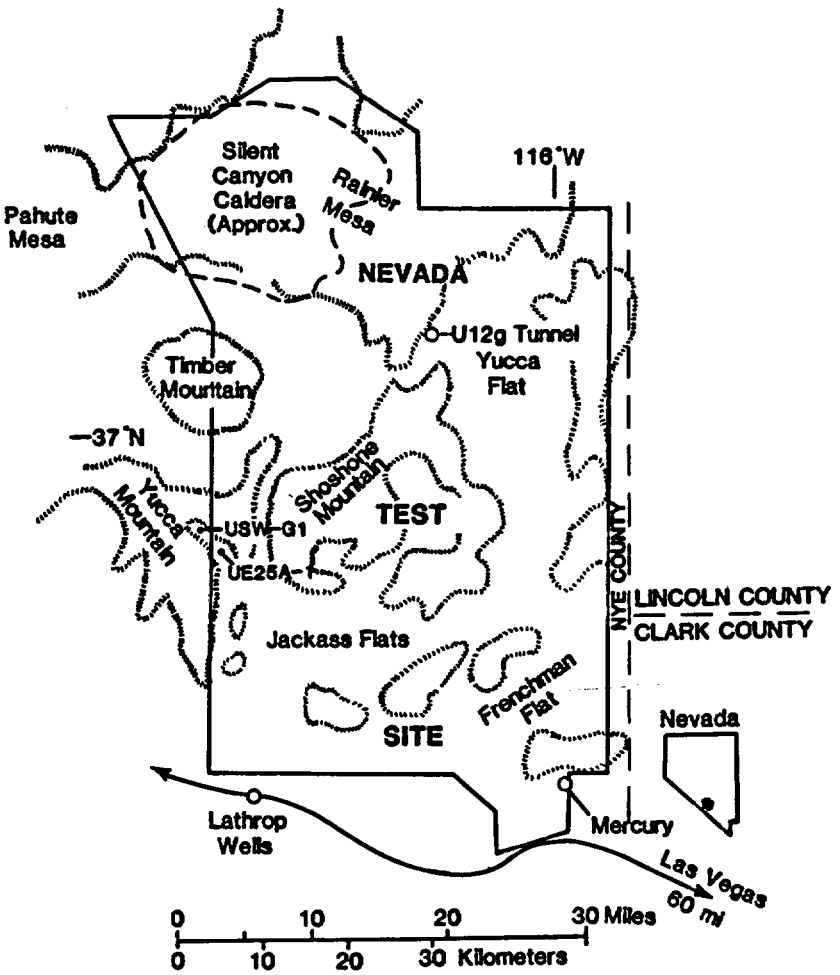

Figure 1. Index Map of Rainier Mesa and Vicinity, Nye County, NV

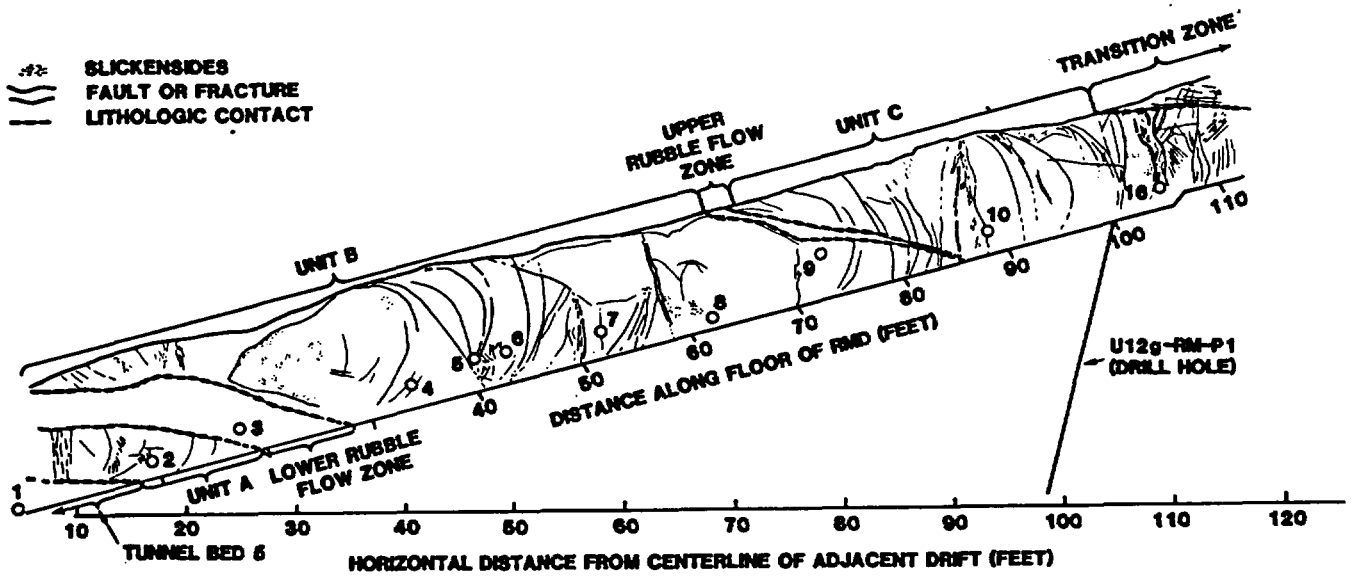

Figure 2. Sketch Map of Left Rib of RMD, Showing RMD Sample Locations and Stratigraphic Contacts Between Informal Stratigraphic Units (Modified from Ref 2)

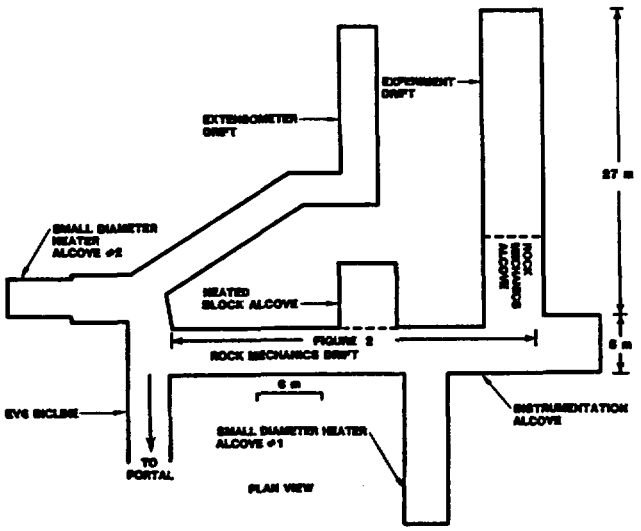

Figure 3. Simplified Plan View of Part of the G-Tunnel Facility as of September 1982

The Grouse Canyon Member in G-Tunnel consists of three separate flow units, separated by volcanic rubble flow zones of variable thickness. From the base upward, the flow units are informally designated in this report as Units A, B, and C.

Unit A is a pale greenish-brown, phenocryst-poor ash-flow (sometimes termed the "basal vitrophyre") about 1.5 m (5 ft) thick, which fractures somewhat conchoidally. It is largely devitrified and densely welded. In the RMD, this unit is overlain by a rubble flow zone 1 to 2 m (3 to 6 ft) thick, in which the matrix is composed primarily of reddish-brown clay. In the RMD, the rubble flow zone contains abundant rounded cobbles of volcanic and plutonic material; these cobbles are often 5 cm or more in diameter. Hole U12g-RM-P1 intersects this horizon at a distance of about 30 m (100 ft) down-dip. In U12g-RM-P1 the rubble flow is less than 1 m (3 ft) thick, and the matrix is tuffaceous and very well cemented.

Unit B is an ash-flow about 6 m (20 ft) thick, in which both compositional and welding zonation is apparent. Color varies from pale reddish-brown near the base to brick-red near the center and brownish-gray near the top. Most of the unit is moderately welded, except for the densely welded, brick-red middle part. The variable degree of welding is indicated by variable flattening of pumice fragments (schlieren or fiamme), by overall color, and by variable bending of shards and matrix around crystal and rock fragments. Unit B is overlain in the RMD by a rubble flow zone up to 0.6 m (2 ft) thick; this zone thins to several centimetres down-dip within the drift and was not intersected in Hole U12g-RM-P1. Except for smaller clast size and a somewhat more indurated matrix, this unit is similar to the rubble flow zone overlying Unit A.

Unit C is a dark-brown, moderately to slightly welded ashflow about 5 m (15 ft) thick. The degree of welding decreases upward through the unit. In its lower part it is similar to the upper part of Unit B; undeformed pumice is common in its upper part. In general, phenocrysts appear more abundant in Unit C than in underlying units, as are argillaceous pumice and rock fragments.

The Grouse Canyon Member is highly fractured in the RMD. Although not described in detail here, fractures mapped in the drift (Figure 2) are generally curvilinear and are rarely traceable for more than a few metres. The upper part of Unit C is most intensely fractured and is cut by two faults. One fault intersects the drift at a high angle at about 27 m (88 ft) (Figure 2) and contains brecciated tuff in a reddish-brown matrix. The second intersects the drift at about 32 m (105 ft) and includes a breccia zone up to 0.6 m (2 ft) wide, containing a central clay-rich gouge zone; the gouge zone strikes about E-W. Many subhorizontal slickensides are present in both ribs of the drift and are most evident on surfaces approximately parallel to the strike of the drift (N35°W). Additional details are contained in the report by Langkopf and Eshom.[2]

Bulk Chemistry

The Grouse Canyon Member of the Belted Range Tuff is broadly peralkaline in nature (molecular $(Na_2O+K_2O)/Al_2O_3 \geq 1$). The Topopah Spring Member, in contrast, is part of a subalkaline calc-alkalic volcanic series, in which molecular $(Na_2O+K_2O)/Al_2O_3$ is less than 1.[4] Available bulk chemical data for the Grouse Canyon Member are summarized in this section.

Noble et al[5] present petrologic and geochemical data on rocks erupted from the Silent Canyon volcanic center (Figure 1), including the Grouse Canyon Member (Table 1, Analyses 1 and 2). Noble[6] suggests that significant amounts of sodium and other volatile elements were lost from the Grouse Canyon Member during postemplacement hydration and crystallization. Most of the evidence for this interpretation is derived from comparison of major-element analyses of nonhydrated, devitrified, and crystallized samples assumed to have the same initial bulk composition (Table 1, Analyses 1, 3-5, versus Analyses 2, 6-18). The average Na_2O content and molecular alkali-alumina ratio average 5.37 ± 0.04 wt% and 1.19 ± 0.023 for nonhydrated glasses assumed near original bulk composition, compared to 4.56 ± 0.33 wt% and 1.105 ± 0.045, respectively, for devitrified samples.

Analyses of the Grouse Canyon Member contained in Table 1 indicate that these rocks are comendites; i.e., high-silica, alkali-rich rhyolites (molecular Al_2O_3 less than $Na_2O + K_2O$) that are not very iron-rich. In general, such rocks have more Na, Fe, F, and Cl than do calc-alkalic rhyolites with similar Si contents, but less Al, Mg, and Ca.

Crowe and Sargent[7] plot major-element variation diagrams for 154 volcanic rocks from the Silent Canyon Center, including 27 samples from the Grouse Canyon Member. The data presentation, however, does not separate samples of the Grouse Canyon Member from those of the Tub Spring Member of the Belted Range Tuff, which is also peralkaline.[1] The alkali-alumina data of Crowe and Sargent[7] indicate that nonhydrated glasses from the Grouse Canyon and Tub Spring Members have peralkalinity ratios (molecular$(Na_2O+K_2O)/Al_2O_3$) ranging from ~0.94 to 1.19, lower than indicated by the data of Noble.[5,6] Crystalline samples considered by Crowe and Sargent[7] are variable in composition, with peralkalinity ratios ranging approximately from 0.84 to 1.22. The distribution between these extremes is fairly even, with 27 of the reported analyses having a ratio of 1 or greater, and 24 a ratio of less than 1. The average ratio for all samples would be only slightly greater than 1. Thus, crystalline samples from the Grouse Canyon and Tub Spring Members do appear to be distinctly less peralkaline than vitric samples, as originally suggested by Noble.[6]

Major-element fractionation trends for the Silent Canyon volcanics and other peralkaline volcanic suites suggest that comendites originate by partial melting of a Ca, Mg-poor parental trachyte, followed by fractional crystallization. The chief evidence for this is the strong tendency for Na:K ratios to be lower in phenocrysts in comendites than in associated glasses, presumably because of fractionation of anorthoclase feldspar.[8] This is supported by the very low Sr contents of peralkaline glasses, implying protracted fractionation and partitioning of Sr into crystallized feldspars.[9]

Five major and minor element analyses of samples from the three flow units in the Grouse Canyon Member in the RMD are given in Table 2. From these analyses, molecular $(Na_2O+K_2O)/Al_2O_3$ (Table 3), modified molecular norms, and Thornton-Tuttle differentiation indices (Table 4) were calculated. Except for the hydrated and altered sample (RMD-2), the differentiation indices (total normative quartz + orthoclase + albite) are high (Table 4), ranging from 93.9 to 96.2. This suggests a highly differentiated source for the Grouse Canyon Member. Both the extent of peralkalinity and the differentiation index decrease slightly upward within flow Unit B. Most of this variation is caused by a decrease in sodium content and suggests either increasing sodium loss upward or eruption from a zoned magmatic chamber.

Table 1. Bulk Chemical Analyses of the Grouse Canyon Member of the Belted Range Tuff, Compiled From Published Literature

Oxide or Element	Analysis 1	2	3	4	5	6	7	8	9	10	11	12	13	14	15	16	17	18
SiO_2	73.8	74.0	73.98	73.84	73.69	75.14	74.0	75.05	74.5	73.61	73.8	74.4	75.0	74.0	74.6	75.2	73.7	74.7
Al_2O_3	11.3	11.3	11.28	11.80	11.28	11.27	11.5	11.19	11.4	11.07	11.4	11.3	11.2	11.3	11.0	10.8	11.7	11.3
Fe_2O_3	1.7	2.5	1.71	1.01	1.83	2.27	3.5	1.78	2.3	3.70	2.6	3.1	3.2	2.2	3.3	3.3	2.5	3.4
FeO	1.8	1.0	1.80	2.07	1.74	1.33	0.05	0.92	1.4	–	1.1	0.61	0.55	1.3	0.10	0.06	1.1	0.05
MgO	0.02	0.1	0.01	0.03	0.01	0.04	0.03	–	–	0.14	0.10	0.07	0.05	0.18	0.22	0.19	0.14	0.13
CaO	0.25	0.3	0.24	0.29	0.21	0.25	0.14	0.11	0.37	0.49	0.09	0.10	0.16	0.29	0.46	0.44	0.11	0.29
Na_2O	5.4	4.8	5.33	5.40	5.35	4.88	4.5	5.09	4.8	4.79	4.6	4.7	4.2	4.6	4.1	4.1	4.8	4.1
K_2O	4.5	4.6	4.55	4.50	4.35	4.57	4.7	4.67	4.5	4.56	4.8	4.4	4.4	4.5	4.5	4.4	4.6	4.9
H_2O^+	0.2	0.4	0.16	0.17	0.43	0.12	0.66	0.15	0.48	0.31	0.62	0.28	0.65	0.45	0.81*	0.84*	0.49*	0.69*
H_2O^-	–	–	0.02	0.01	0.01	0.18	0.15	0.11	0.17	0.31	0.36	0.14	0.11	0.12	–	–	–	–
TiO_2	0.22	0.22	0.22	0.22	0.22	0.22	0.20	0.22	0.22	0.22	0.23	0.22	0.24	0.21	0.22	0.21	0.20	0.21
ZrO_2	0.13	0.13	–	–	–	–	–	–	–	–	–	–	–	–	–	–	–	–
MnO	0.17	0.17	0.17	0.17	0.17	0.18	0.17	0.17	0.17	0.14	0.17	0.14	0.14	0.15	0.17	0.16	0.18	0.15
P_2O_5	0.01	0.02	0.01	0.01	0.01	0.01	0.03	0.01	0.08	0.03	0.04	0.06	0.04	0.05	0.01	0.01	0.04	0.01
CO_2	<0.01	0.05	0.02	0.01	–	0.09	<0.05	0.02	<0.05	0.12	<0.05	<0.05	<0.05	<0.05	<0.05	<0.05	<0.05	0.07
Cl	0.12	0.02	0.13	0.11	0.11	0.01	–	0.02	–	0.03	0.03	–	–	0.03	–	–	–	–
F	0.17	0.07	0.17	0.16	0.17	0.10	–	0.09	–	0.03	0.10	0.08	0.05	0.11	–	–	–	–
Subtotal	100.	100.	100.05	100.06	100.01	99.86	–	99.83	–	99.80	–	–	–	–	–	–	–	–
Less O	−0.10	−0.03	0.10	0.10	0.10	0.04	–	0.04	–	0.02	–	–	–	–	–	–	–	–
TOTAL	100.	100.	99.95	99.96	99.91	99.82	100.	99.79	100.	99.78	100.	100.	100.	99.	100.	100.	100.	100.
Molecular (Na_2O+K_2O) /Al_2O	1.217	1.139	1.214	1.166	1.197	1.151	1.086	1.200	1.120	1.157	1.119	1.105	1.04	1.100	1.056	1.065	1.100	1.066

Analysis
1: nonhydrated glasses from lower part of Member (Noble et al)[6]
2: densely welded, primarily crystallized ash-flow tuff from lower part of Member (Noble et al)[6]
3,4,5: aphyric nonhydrated glasses from lowermost part of Member (Noble)[6]
6,7,8,9,12,13: densely welded and granophyrically crystallized ash-flow tuff (Noble)[6]
10: partly welded and devitrified ash-flow (Noble)[6]
11,14,15,16,17,18: densely welded and devitrified ash-flow tuff (Noble)[6]

Notes:
– = below analytical limit
na = not analyzed
* = total H_2O (H_2O^+ and H_2O^-)

Table 2. Bulk Chemical Analyses of the Grouse Canyon Member, RMD Samples*

	Sample				
	RMD-2	RMD-4	RMD-6	RMD-9	RMD-10
Analysis	1	2	3	4	5
Informal Unit	A	Lower B	Middle B	Upper B	C
Oxide					
SiO_2	64.26	74.73	71.33	72.83	73.63
Al_2O_3	11.66	11.25	13.00	11.8	12.16
Fe_2O_3	3.38	2.50	2.46	2.24	2.65
FeO	0.40	1.13	1.60	2.51	0.73
MgO	0.26	0.06	0.06	0.10	0.05
CaO	2.07	0.19	0.33	0.36	0.18
Na_2O	2.33	3.40	4.25	3.95	3.47
K_2O	3.24	5.30	5.53	4.84	5.40
$H_2O+(+CO_2)$	6.81	0.54	0.34	0.34	0.79
H_2O-	5.22	0.08	0.08	0.14	0.13
TiO_2	0.18	0.19	0.26	0.235	0.28
P_2O_5	0.01	0.02	0.12	0.04	0.031
MnO	0.156	0.132	0.154	0.148	0.145
SrO	0.003	0.001	0.001	0.001	0.001
SO_3	<0.1	<0.1	<0.1	<0.1	<0.1
TOTAL WT. %	99.98	99.52	99.51	99.53	99.65
Total Fe (as Fe_2O_3)	3.83	3.76	4.24	5.03	3.46
Loss on Ignition	6.77	0.42	0.16	0.06	0.50
FeO after Loss on Ignition	0.0	0.0	0.0	0.0	0.0

*Analyses by John Husler, Department of Geology, University of New Mexico. Analytical technique described in Appendix A.

Table 3. Alkalinity Ratios of Analyzed Samples. Ratio is (molecular Na_2O + molecular K_2O)/(molecular Al_2O_3)

	Sample				
	RMD-2	RMD-4	RMD-6	RMD-9	RMD-10
Informal Unit	A	Lower B	Middle B	Upper B	C
Whole rock	0.629	1.007	0.998	0.994	0.950
Feldspar phenocrysts	0.953	0.928	0.947	0.964	0.883
Glass	1.261	1.222	1.085	1.188	1.060

Table 4. Molecular Norms and Differentiation Indices of Analyzed Samples

		Sample				
Normative Mineral	Symbol	RMD-2	RMD-4	RMD-6	RMD-9	RMD-10
Apatite	ap	0.02	0.04	0.26	0.09	0.07
Ilmenite	il	0.29	0.27	0.37	0.34	0.40
Orthoclase	or	22.36	32.28	33.28	29.34	32.86
Albite	ab	24.44	31.02	38.87	36.39	32.10
Anorthite	an	11.93	–	0.06	0.18	0.71
Acmite	ac	–	0.36	–	–	–
Corundum	C	0.74	–	–	–	0.40
Magnetite	mt	1.08	2.56	2.62	2.40	1.50
Hematite	hm	2.04	–	–	–	0.91
Diopside	di	–	0.42	0.65	1.11	–
Enstatite	en	0.84	–	0.10	0.22	0.14
Ferrosilite	fs	–	–	0.40	1.80	–
Wollastonite	wo	–	0.13	–	–	–
Quartz	q	36.26	32.92	23.40	28.14	30.92
TOTAL		100.01	100.01	100.01	100.00	100.00
DI*		83.06	96.22	95.55	93.87	95.88

*DI is the Thornton-Tuttle differentiation index (normative q+ab+or).

Except for the hydrated and altered sample from Unit A (RMD-2), the samples lie very near the subalkaline-peralkaline boundary ($(Na_2O+K_2O)/Al_2O_3 = 1$). The alkali-alumina ratio for whole-rock analyses ranges only from 0.950 to 1.007. Thus, the samples are less peralkaline than those reported by Noble,[5,6] but are well within the range of values reported by Crowe and Sargent[7] for crystalline rocks of the Silent Canyon Center.

Petrography

Petrographic characteristics of several representative samples collected for this study are summarized here, in an overview of the general textures and mineralogies in the welded Grouse Canyon Member. Detailed descriptions of individual samples are contained in Appendix B.

The upper portion of Tunnel Bed 5 (Sample RMD-1, Figure 2), which underlies the Grouse Canyon Member, is composed chiefly of undeformed to slightly flattened pumice fragments, constituting about 70% of the mode (Figure 4). Five percent of the rock consists of zeolitized perlite fragments, and <5% of recognizable individual glass shards. Pore space is present both between and within pumice fragments. The abundance of uncollapsed pumice and the very weak preferred orientation of individual shards indicate that the rock is nonwelded to very slightly welded, or has undergone slight diagenetic compaction. Both matrix and pumice fragments in upper Tunnel Bed 5 appear isotropic when viewed at low magnification but are seen to be very finely crystalline (<5 micron crystals) at higher magnification. This material includes crystalline, low-relief, low-birefringence crystals (clinoptilolite) and reddish-brown translucent crystal aggregates <0.05 mm in diameter (iron-manganese oxides?). Concentric rings of low-relief minerals (chiefly clinoptilolite) are present in pores within altered perlite. No phenocrysts are present in sections examined from this zone.

The ash-flow tuff of Unit A, the "basal vitrophyre" (RMD-2), is densely to moderately welded and contains sparse phenocrysts (<3%), dominated by partly resorbed alkali feldspar. Welding is indicated by the strong preferred orientation of the shard matrix and by flattening of pumice fragments (Figure 5). Although the pumice in general is highly devitrified, some deformed pore space remains in many fragments. The rock is dominated by shards and pumice and contains ~2% volcanic argillaceous rock fragments. Glass shards are only partially devitrified.

Figure 4. Photomicrograph of Sample RM-P1-53.8 From Upper Tunnel Bed 5, Showing Slightly Deformed Pumice (Transmitted, plane-polarized light. Width of field of view is 2.9 mm.)

Clasts in the rubble flow zone overlying Unit A are dominantly subrounded pebbles or cobbles of reddish-brown to brown ash-flow tuff, with subordinate fine-grained granitic and argillaceous fragments. In the RMD (RMD-3) the matrix is reddish-brown clay; in Hole U12g-RM-P1 (RMP-P1-30) the matrix consists of slightly welded, poorly crystallized glass shards, plus some alkali feldspar phenocrysts and small lithic fragments. The clay matrix in the rubble flow zone exposed in the drift is thus apparently secondary.

The rubble flow is also thicker in the drift than in nearby holes or exposures, suggesting that it was deposited in a topographic low, and is therefore a likely horizon for "ponding" of groundwater, perhaps leading to extensive alteration in both the rubble flow zone and underlying Unit A. Bulk chemical data for welded tuff from Unit A (RMD-2), given in Table 2, show an excess of uncombined water (H_2O^-), much more CaO, and less SiO_2 than do analyses of other samples of the Grouse Canyon (Tables 1 and 2). These

differences are compatible with alteration of the lowest part of the member by groundwater moving downward through the rubble flow zone between Units A and B.

Figure 5. Photomicrograph of Sample RMD-2 From Unit A, Showing Moderately to Densely Welded Texture, as Indicated by Preferred Orientation of Shards (Transmitted, plane-polarized light. Width of field of view is 2.9 mm.)

Unit B was sampled (RMD-4, 6, 7, and 9) and examined in more detail than the other units because it shows the most variation in welding, phenocryst content, and degree of crystallization. The lowest part of the unit is moderately welded (Figure 6, RMD-4) and contains rare, slightly flattened pumice and common elongate crystalline areas. These areas may represent flattened pumice crystallized following welding. The lower part of Unit B contains 6% to 8% total phenocrysts, almost exclusively alkali feldspar, and is less densely welded than parts of Unit A.

Figure 6. Photomicrograph of Sample RMD-4 From Lower Part of Unit B, Showing Somewhat Lesser Welding Than Unit A (Figure 5) (Transmitted, plane-polarized light. Width of field of view is 2.9 mm.)

The middle part of Unit B (RMD-6, 7) is brick-red and densely welded (Figure 7). Pumice is very flattened, with almost total loss of porosity (fiamme structure). After flattening, the fiamme crystallized. Shards in the matrix show a very strong preferred orientation and are commonly bent around rock fragments and phenocrysts. Alkali feldspar is the dominant phenocryst (8% to 12%) and is commonly embayed, with crystallization common in embayments. Anhedral quartz is a subordinate phenocryst phase. Axiolitic devitrification of shards is common; devitrification minerals appear to be finely intergrown alkali feldspar and quartz, although some tridymite or cristobalite may be present. The red color in hand specimen is apparently caused by very tiny, disseminated

grains of iron oxide (hematite) in the shard-rich matrix. Rock fragments in this zone are predominantly volcanic in origin and are composed of small alkali feldspar phenocrysts in a recrystallized (axiolitic to spherulitic) matrix; fragments of argillaceous sedimentary rocks are subordinate.

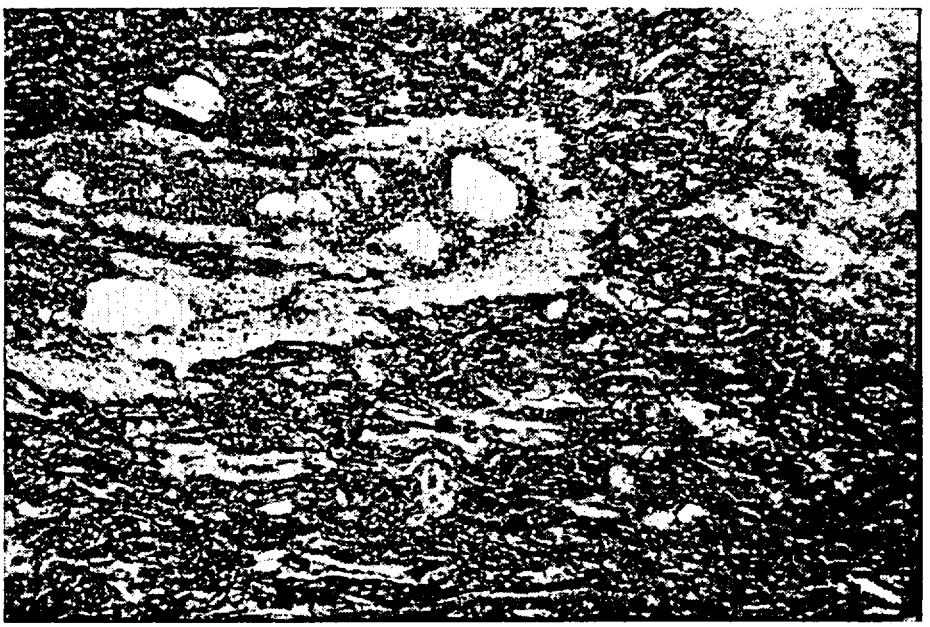

a. Plane – Polarized Light

b. Crossed Polarizers

Figure 7. Photomicrograph of Sample RMD-6 From Middle Part of Unit B, Showing Welding and Crystallization. Densely welded ash-flow tuff containing flattened, devitrified pumice and shards with local bending of matrix around rock fragments and crystals (Transmitted light. Width of field of view is 2.9 mm.)

The upper part of Unit B (RMD-9) is moderately welded and generally brownish-gray in color. Pumice is commonly elongate and crystallized, but flattened bubbles are present in many fragments. Total phenocryst content is similar to that in the underlying tuff but includes some quartz (~1%). The matrix is strongly devitrified, and shard texture is partly obliterated by crystallization. Overall, Unit B shows a normal or nearly symmetrical welding zonation,[10] an upward increase in degree of crystallization of the matrix from ~50% to nearly 100%, and an upward increase in phenocryst content from 8% to 14%.

Units B and C are separated by a thin, intermittent rubble flow zone, not studied in detail. Unit C (RMD-10) is moderately to slightly welded and has a more granular appearance in thin section than the more densely welded tuffs below (Figure 8) because of coarser devitrification and common vapor-phase crystallization. Total phenocryst content is about the same as in the underlying upper part of Unit B, but quartz is more abundant. The unit is more extensively crystallized than are comparably welded zones from underlying units. Devitrification is axiolitic and spherulitic in larger shards and pumice clasts, and the shard-rich matrix is almost completely altered to a mix of small, low-birefringent crystals of quartz and alkali feldspar, yellowish granules showing high relief and dark, high-relief, isotropic to opaque crystals. Matrix crystallization appears to have followed welding and crystallization of pumice and shards.

a. Plane – Polarized Light

Figure 8. Photomicrograph of Sample RMD-10 From Unit C, Showing Welding and Crystallization. Slightly welded ash-flow tuff containing slightly deformed pumice and extensively crystallized matrix that obscures shard texture (Transmitted light. Width of field of view is 2.9 mm.)

b. Crossed Polarizers

Figure 8. Concluded

Figure 9. Photomicrograph of Sample RMD-11 From Transition Zone, Showing Moderate Welding and Much More Pronounced Size Sorting Than the Grouse Canyon Samples (Figures 3 to 7) (Transmitted, plane-polarized light. Width of field of view is 2.9 mm.)

The Transition Zone above Unit C (RMD-11) is a moderately welded ash-flow tuff. In comparison with the Grouse Canyon Member, this tuff is well-sorted and contains few crystals, pumice, or rock fragments larger than 1 mm (Figure 9). Rock fragments in this zone include some cherty sediments and metamorphic(?) rocks not found in the Grouse Canyon Member. In addition, some feldspar phenocrysts are plagioclase, which is notably absent from the Grouse Canyon Member. The Upper Transition Zone thus appears to represent the distal portion of an overlying ash-flow sheet that may not be related to the Grouse Canyon Member.

Analytical Mineralogy

Feldspars, mafic silicates, oxides, and glasses in all tuff samples were analyzed by electron microprobe in order to provide detailed characterization support for thermomechanical experiments and to serve as a basis for detailed comparison of the welded Grouse Canyon Member with the Topopah Spring Member. Quantitative analyses were made with an automated ARL-EMX SM electron microprobe by means of wavelength-dispersive analysis. The microprobe was operated at a 15-kV acceleration potential and at varying sample currents, depending on the phases analyzed. A broad (10-μm) beam was used to minimize volatilization of alkalis during analyses of feldspars and glasses. Oxide weight percentages reported in the data tables (Tables 5 to 9) are those calculated after correction by the Bence-Albee scheme[11] and are believed precise to $\pm 1\%$ of the amounts reported. Sample identifications and locations within individual thin sections are on file at the Institute of Meteoritics, University of New Mexico.

Table 5a. Microprobe Analyses of Feldspars, Sample RMD-2

	Analysis													
	1		2		3		4		5		6		7	
Crystal ID:	F-1a		F-2a		rF-3a		PF-4a		F-5a		F-1b		rF-3b	
Oxide	c	e	c	e	c	e	c	e	c	e	c	e	c	e
SiO_2	65.7	65.7	67.0	67.1	65.8	68.4	66.0	66.4	66.9	66.6	66.4	66.6	68.0	67.5
Al_2O_3	20.0	19.6	18.9	18.4	19.8	18.6	18.8	18.1	19.0	18.5	18.2	18.4	18.1	17.6
FeO	0.18	0.23	0.27	0.24	0.21	0.44	0.29	0.32	0.26	0.30	0.20	0.25	0.47	0.28
MgO	nd	nd	nd	nd	nd	nd	nd	0.02	nd	nd	nd	nd	nd	nd
CaO	0.43	0.48	0.01	0.07	0.85	1.18	0.61	0.50	0.33	0.20	0.61	0.55	0.04	0.15
Na_2O	6.7	6.5	6.5	6.7	6.1	3.20	4.99	5.86	6.9	7.0	6.4	6.3	7.4	7.4
K_2O	7.2	7.0	7.4	7.3	7.0	7.2	7.7	7.6	6.3	6.3	6.6	6.8	5.89	5.65
TOTAL WT%	100.2	99.5	100.1	99.8	99.8	99.0	98.4	98.8	99.7	98.9	98.4	98.9	99.9	98.6

	Average Weight Percent			
	Core	Range	Edge	Range
SiO_2	66.6	(65.7-68.5)	66.9	(65.7-68.4)
Al_2O_3	19.0	(18.1-20.0)	18.5	(17.6-19.6)
FeO	0.27	(0.18-0.47)	0.29	(0.23-0.44)
MgO	nd	(----------)	0.0	(0.00-0.02)
CaO	0.41	(0.01-0.85)	0.45	(0.07-1.18)
Na_2O	6.4	(4.99-6.9)	6.1	(3.20-7.4)
K_2O	6.9	(5.89-7.7)	6.8	(5.89-7.6)
TOTAL	99.6		99.0	

Nomenclature:

F-1a = Feldspar #1, Probe Section a
c = core analysis
e = edge analysis (within 20 microns of grain edge)
nd = not detected
r = resorbed phenocryst
P = within pumice clast

Table 5b. Microprobe Analyses of Feldspars, Sample RMD-4

	Analysis												
	1		2		3		4		5		6	7	
Crystal ID:	F-1a		rF-3a		F-1b		F-2b		F-3b		F-5b	F-6b	
Oxide	c	e	c	e	c	e	c	e	c	e	c	c	e
SiO_2	67.7	68.0	68.4	69.0	68.2	67.3	65.7	67.1	66.8	66.9	67.1	68.3	68.7
Al_2O_3	19.6	19.5	19.4	19.5	18.8	19.2	19.2	19.3	19.5	19.8	20.1	19.4	19.5
FeO	0.18	0.19	0.19	0.17	0.20	0.24	0.17	0.20	0.16	0.23	0.06	nd	nd
MgO	nd	nd	nd	nd	nd	nd	nd	nd	nd	nd	0.01	nd	nd
CaO	0.37	0.40	0.13	0.13	0.08	0.15	0.60	0.54	0.95	0.97	0.62	0.48	0.40
Na_2O	6.3	6.2	7.2	6.6	6.8	7.2	6.2	6.2	6.0	6.3	6.8	6.4	6.2
K_2O	7.2	7.0	6.3	6.5	6.5	6.3	6.5	6.8	6.9	6.8	6.5	7.3	7.2
TOTAL WT%	101.4	101.3	101.6	101.5	100.6	100.4	98.4	100.1	100.3	101.0	101.2	101.9	102.0

	Average Weight Percent			
	Core	Range	Edge	Range
SiO_2	67.5	(65.7-68.4)	67.8	(66.9-69.0)
Al_2O_3	19.4	(18.8-20.1)	19.5	(19.2-19.8)
FeO	0.14	(0.0-0.20)	0.17	(0.0-0.24)
MgO	nd	(----------)	0.0	(0.0-0.01)
CaO	0.46	(0.08-0.95)	0.43	(0.13-0.97)
Na_2O	6.5	(6.0-7.2)	6.5	(6.2-7.2)
K_2O	6.7	(6.3-7.3)	6.8	(6.3-7.2)
TOTAL	100.7		101.2	

Nomenclature:

F-1a = Feldspar #1, Probe Section a
c = core analysis
e = edge analysis (within 20 microns of grain edge)
nd = not detected
r = resorbed phenocryst

Table 5c. Microprobe Analyses of Feldspars, Sample RMD-6

	Analysis												
	1		2		3		4		5	6	7	8	9
Crystal ID:	F-2a		F-3a		F-4a		F-5a		PF-7a	F-8a	*F-11a	rF-1b	*F-5b
Oxide	c	e	c	e	c	e	c	e	c	c	c	c	c
SiO_2	67.2	67.3	67.6	66.9	67.3	65.3	65.2	64.9	68.1	68.0	68.5	67.0	67.5
Al_2O_3	20.3	20.2	20.0	19.1	19.9	19.9	20.9	20.8	19.0	18.6	18.3	19.3	19.5
FeO	0.33	0.21	0.27	0.30	0.25	0.18	0.13	0.20	0.32	0.24	0.10	0.26	0.33
MgO	nd	nd	nd	nd	nd	0.20	0.12	0.05	nd	nd	nd	nd	nd
CaO	0.35	0.34	0.27	0.13	0.43	0.38	0.81	0.98	0.22	0.13	0.12	0.66	0.51
Na_2O	6.7	7.0	7.4	7.2	7.00	6.9	6.5	8.2	7.0	6.4	4.28	6.4	4.23
K_2O	6.9	6.8	6.3	6.8	6.9	6.7	7.0	6.7	6.7	7.5	10.6	7.5	9.5
TOTAL WT%	101.8	101.8	101.8	100.4	101.8	99.6	100.7	101.8	101.3	100.9	101.9	101.1	101.6

	Average Weight Percent, Excluding Analyses 7 and 9				Average Weight Percent Analyses 7 and 9
	Core	Range	Edge	Range	
SiO_2	67.2	(65.2-68.1)	66.1	(64.8-67.3)	68.0
Al_2O_3	19.7	(18.6-20.9)	20.0	(19.1-20.8)	18.9
FeO	0.26	(0.13-0.33)	0.22	(0.18-0.30)	0.30
MgO	0.02	(0.0-0.12)	0.06	(0.0-0.20)	nd
CaO	0.41	(0.13-0.81)	0.46	(0.13-0.98)	0.32
Na_2O	6.8	(6.4-7.4)	7.4	(6.9-8.2)	4.26
K_2O	7.0	(6.3-7.5)	6.7	(6.7-6.8)	10.0
TOTAL	101.3		100.9		101.8

Table 5d. Microprobe Analyses of Feldspars, Sample RMD-7

	Analysis												
	1		2		3	4	5	6		7		8	
Crystal ID:	F-1a		rF-2a		F-3a	F-4a	*F-5a	F-6a		F-8a		F-9a	
Oxide	c	e	c	e	c	c	c	c	e	c	e	c	e
SiO_2	67.2	66.6	66.2	66.9	66.5	66.8	67.8	68.0	67.4	66.9	65.7	67.4	67.3
Al_2O_3	18.7	18.8	19.6	19.8	19.5	19.2	19.0	18.9	19.3	19.7	19.4	19.5	19.5
FeO	0.31	0.32	0.25	0.30	0.22	0.21	0.18	0.13	0.17	0.23	0.25	0.19	0.27
MgO	nd	nd	nd	nd	0.03	0.09	0.10	nd	0.08	0.01	0.02	nd	0.05
CaO	0.07	0.07	0.87	0.84	0.76	0.36	0.17	0.18	0.17	0.94	0.91	0.60	0.52
Na_2O	7.6	7.4	6.7	6.9	7.3	7.0	7.2	6.5	7.0	7.2	6.6	6.5	6.7
K_2O	6.5	6.6	7.0	6.9	6.8	7.3	7.1	7.7	7.4	7.0	7.1	7.6	7.5
TOTAL WT%	100.4	99.8	100.6	101.6	101.1	101.0	101.6	101.4	101.5	102.0	100.0	101.8	101.8

Average Weight Percent, Excluding Analysis 5

	Core	Range	Edge	Range
SiO_2	67.0	(66.2-68.0)	66.8	(65.7-67.4)
Al_2O_3	19.3	(18.7-19.7)	19.4	(18.8-19.7)
FeO	0.22	(0.13-0.31)	0.26	(0.18-0.32)
MgO	0.01	(0.0-0.03)	0.03	(0.0-0.10)
CaO	0.54	(0.07-0.94)	0.50	(0.07-0.91)
Na_2O	7.0	(6.5-7.2)	6.9	(6.6-7.4)
K_2O	7.1	(6.5-7.7)	7.1	(6.6-7.5)
TOTAL	101.2		101.0	

Nomenclature:

F-1a = Feldspar #1, Probe Section a
c = core analysis
e = edge analysis (within 20 microns of grain edge)
nd = not detected
r = resorbed phenocryst
* = average of multiple analysis of feldspars in xenolithic clasts

Table 5e. Microprobe Analyses of Feldspars, Sample RMD-9

	Analysis											
	1		2		3		4		5	6	7	8
Crystal ID:	F-1a		F-2a		F-4a		F-5a		rF-7a	*F-8a	PF-3b	PF-4b
Oxide	c	e	c	e	c	e	c	e	c	c	c	c
SiO_2	67.4	68.3	67.4	67.7	67.5	66.8	67.6	67.8	66.5	66.1	67.9	67.1
Al_2O_3	19.6	19.6	19.2	19.2	18.9	19.5	19.5	19.7	19.6	20.7	18.8	18.6
FeO	0.25	0.26	0.21	0.20	0.21	0.29	0.17	0.29	0.24	0.24	0.18	0.22
MgO	nd	0.01	nd	nd	nd	nd	nd	nd	nd	nd	0.19	0.17
CaO	0.52	0.54	0.55	0.25	0.71	0.73	0.60	0.71	0.48	1.00	0.08	0.17
Na_2O	6.7	6.7	6.7	5.8	5.8	6.1	6.3	6.3	7.1	6.3	7.8	7.0
K_2O	6.8	6.5	6.3	7.8	7.4	7.4	6.8	6.8	6.7	6.6	6.4	7.1
TOTAL WT%	101.3	101.9	100.4	101.0	100.5	100.8	101.0	101.6	100.6	100.9	101.4	100.4

Average Weight Percent, Excluding Analyses 6, 7, and 8

	Core	Range	Edge	Range
SiO_2	67.3	(66.5-67.9)	67.6	(66.8-68.3)
Al_2O_3	19.2	(18.6-19.6)	19.5	(19.2-19.7)
FeO	0.21	(0.17-0.25)	0.26	(0.20-0.29)
MgO	0.04	(0.0-0.19)	nd	(----------)
CaO	0.44	(0.17-0.71)	0.55	(0.25-0.73)
Na_2O	6.8	(5.8-7.8)	6.2	(5.8-6.7)
K_2O	6.8	(6.3-7.4)	7.1	(6.5-7.7)
TOTAL	100.8		101.2	

Nomenclature:

F-1a = Feldspar #1, Probe Section a
c = core analysis
e = edge analysis (within 20 microns of grain edge)
nd = not detected
r = resorbed phenocryst
* = average of multiple analysis of feldspars in xenolithic clasts
P = within pumice clast

Table 5f. Microprobe Analyses of Feldspars, Sample RMD-10

	Analysis										
	1		2		3		4		5		6
Crystal ID:	PF-1a		F-2a		F-3a		rF-4a		F-5a		rF-6a
Oxide	c	e	c	e	c	e	c	e	c	e	e
SiO_2	66.1	66.3	65.1	65.2	65.6	65.5	65.4	65.9	66.1	66.0	64.7
Al_2O_3	19.3	19.1	19.9	19.9	19.7	19.9	19.7	19.7	19.8	19.6	20.7
FeO	0.27	0.25	0.22	0.24	0.23	0.25	0.20	0.24	0.23	0.25	0.27
MgO	nd	nd	nd	nd	nd	nd	nd	nd	nd	nd	nd
CaO	0.12	0.16	0.61	0.76	0.67	0.75	0.69	0.60	0.37	0.45	1.56
Na_2O	6.6	6.2	5.58	5.82	5.89	5.67	5.85	5.62	6.3	6.3	6.3
K_2O	6.2	6.8	7.2	7.1	6.8	7.2	7.3	7.4	6.7	6.5	5.43
TOTAL WT%	98.6	98.8	98.6	99.0	98.9	99.3	99.1	99.5	99.5	99.1	99.0

	Average Weight Percent			
	Core	Range	Edge	Range
SiO_2	65.7	(65.1-66.1)	65.5	(64.7-66.3)
Al_2O_3	19.7	(19.2-19.9)	19.8	(19.1-20.7)
FeO	0.23	(0.20-0.27)	0.25	(0.24-0.27)
MgO	nd	(----------)	nd	(----------)
CaO	0.49	(0.12-0.69)	0.71	(0.16-1.56)
Na_2O	6.1	(5.6-6.6)	6.0	(5.6-6.3)
K_2O	6.8	(6.2-7.3)	6.7	(6.8-7.4)
TOTAL	99.0		99.0	

Nomenclature:

F-1a = Feldspar #1, Probe Section a
c = core analysis
e = edge analysis (within 20 microns of grain edge)
nd = not detected
r = resorbed phenocryst
P = within pumice clast

Table 5g. Microprobe Analyses of Feldspars, Sample RMD-11

	Analysis													
	1		2		3		4		5		6		7	8
Crystal ID:	F-1a		F-2a		F-3a		F-4a		F-5a		rF-6a		F-7a	F-8a
Oxide	c	e	c	e	c	e	c	e	c	e	c	e	c	c
SiO_2	66.8	64.4	66.9	67.7	65.7	67.1	67.3	67.1	67.3	66.4	65.6	64.8	61.2	66.2
Al_2O_3	19.6	20.9	19.8	19.9	19.9	19.8	19.8	20.0	19.7	20.1	21.6	21.8	25.8	19.6
FeO	0.22	0.31	0.24	0.26	0.21	0.27	0.20	0.22	0.19	0.29	0.28	0.30	0.31	0.09
MgO	nd	nd	nd	nd	nd	nd	nd	nd	nd	nd	nd	nd	nd	nd
CaO	0.42	1.38	0.68	0.68	0.59	0.56	0.62	0.64	0.56	0.81	2.20	2.58	6.8	0.21
Na_2O	6.3	6.2	6.0	6.2	6.2	6.2	6.1	6.2	5.61	5.93	6.3	6.6	6.9	3.30
K_2O	7.2	6.6	6.9	7.0	7.4	7.4	7.2	7.2	7.9	7.4	5.23	4.68	0.76	11.4
TOTAL WT%	100.5	99.8	100.5	101.7	100.0	101.3	101.2	101.4	101.3	100.9	101.2	100.8	101.8	100.8

	Average Weight Percent			
	Core	Range	Edge	Range
SiO_2	66.6	(65.6-67.3)	66.3	(64.4-67.7)
Al_2O_3	20.1	(19.6-21.6)	20.4	(19.8-21.8)
FeO	0.22	(0.19-0.28)	0.28	(0.22-0.31)
MgO	nd	(----------)	nd	(----------)
CaO	0.85	(0.42-2.20)	1.11	(0.56-2.58)
Na_2O	6.1	(5.6-6.3)	6.2	(5.9-6.3)
K_2O	7.0	(5.2-7.9)	6.7	(4.7-7.4)
TOTAL	100.9		101.0	

Nomenclature:

F-1a = Feldspar #1, Probe Section a
c = core analysis
e = edge analysis (within 20 microns of grain edge)
nd = not detected
r = resorbed phenocryst

Table 5h. Microprobe Analyses of Feldspars, Sample RM-P1-3.0-3.5

	Analysis													
	1		2		3		4		5	6	7		8	9
Crystal ID:	F-1a		F-2a		F-3a		F-4a		F-6a	F-7a	F-8a		F-9a	PF-10a
Oxide	c	e	c	e	c	e	c	e	c	c	c	e	c	c
SiO_2	66.2	65.7	66.6	65.7	67.3	67.7	65.8	66.6	68.6	67.8	66.2	65.4	67.3	67.1
Al_2O_3	19.9	19.8	20.0	20.0	19.5	19.6	20.3	19.8	17.9	18.3	19.8	19.4	17.5	16.1
FeO	0.25	0.24	0.22	0.22	0.22	0.26	0.19	0.29	1.22	0.50	0.20	0.24	1.29	2.68
MgO	nd	nd	nd	nd	nd	nd	nd	nd	nd	nd	nd	nd	nd	0.01
CaO	0.67	0.89	0.66	0.85	0.29	0.57	1.10	0.73	0.06	nd	0.77	0.90	0.02	0.12
Na_2O	5.50	5.92	5.67	5.92	5.91	6.4	5.85	5.65	6.9	6.3	5.75	5.86	5.46	5.19
K_2O	7.3	7.2	7.8	7.2	6.9	6.7	6.7	7.3	5.53	6.4	7.3	7.2	7.1	7.3
TOTAL WT%	99.8	99.8	100.9	99.9	100.2	101.2	99.9	100.4	100.2	99.3	100.0	99.0	98.7	98.5

	Average Weight Percent				10	
					PrF-5a	
	Core	Range	Edge	Range	c	e
SiO_2	67.0	(65.4-68.6)	66.2	(65.4-67.7)	64.0	64.9
Al_2O_3	18.8	(16.1-20.3)	19.7	(19.3-20.0)	21.4	20.7
FeO	0.75	(0.19-2.68)	0.25	(0.22-0.29)	0.29	0.27
MgO	nd	(----------)	nd	(----------)	nd	nd
CaO	0.41	(0.0-1.10)	0.79	(0.57-0.90)	1.98	1.71
Na_2O	5.83	(5.2-6.8)	5.9	(5.5-6.4)	6.2	6.2
K_2O	6.9	(5.5-7.7)	7.1	(6.7-7.7)	5.24	5.84
TOTAL	99.7		99.9		99.1	99.6

Table 5I. Microprobe Analyses of Feldspars, Sample RM-P1-30.0

	Analysis													
	1		2		3		4		5		6		7	
Crystal ID:	F-1a		F-2a		rF-3a		F-4a		F-6a		F-7a		F-8a	
Oxide	c	e	c	e	c	e	c	e	c	e	c	e	c	e
SiO_2	66.5	67.1	67.9	66.2	63.6	64.8	66.1	65.1	67.6	67.2	67.0	66.5	63.7	68.8
Al_2O_3	18.9	18.8	19.4	18.8	21.9	21.4	20.6	21.3	19.9	19.8	19.4	19.5	19.3	18.1
FeO	0.25	0.31	0.22	0.24	0.29	0.29	0.24	0.26	0.27	0.26	0.27	0.26	0.24	1.45
MgO	nd	nd	nd	nd	nd	nd	nd	nd	nd	nd	nd	nd	nd	nd
CaO	nd	0.07	0.29	0.14	2.80	2.36	1.80	2.45	0.48	0.42	0.23	0.17	0.01	nd
Na_2O	6.6	6.4	6.2	6.2	6.6	6.8	6.6	6.7	5.94	5.68	6.2	6.6	6.3	6.4
K_2O	6.4	6.1	4.97	6.5	3.64	4.07	4.75	4.29	6.9	7.3	6.6	6.3	7.4	6.7
TOTAL	98.7	98.8	99.0	98.1	98.8	99.7	100.1	100.1	101.1	100.7	99.7	99.3	97.0	101.5
WT%														

	Average Weight Percent				8	
					F-8a	
	Core	Range	Edge	Range	c	e
SiO_2	66.2	(63.6-67.9)	66.6	(64.8-68.8)	67.0	66.8
Al_2O_3	19.8	(18.8-21.9)	19.6	(18.1-21.4)	19.2	18.8
FeO	0.25	(0.22-0.29)	0.42	(0.24-1.45)	0.25	0.27
MgO	nd	(----------)	nd	(----------)	nd	nd
CaO	0.13	(0.0-2.80)	0.70	(0.0-2.45)	nd	nd
Na_2O	6.4	(5.9-6.6)	6.4	(5.7-6.8)	6.5	6.4
K_2O	5.97	(3.6-7.0)	6.0	(4.1-7.3)	7.0	6.9
TOTAL	98.8		99.7		100.0	99.2

Table 6. Microprobe Analyses of Pyroxenes, Samples RMD-2 and RMD-9

	Sample				
	RMD-2		RMD-9		
Analysis:	1		2	3	
Crystal ID:	Px-1a		Px-1b	Px-2b	
Oxide	c	e	c	c	e
SiO_2	50.9	50.7	50.4	50.1	50.1
TiO_2	0.67	0.72	0.66	0.62	0.61
Al_2O_3	0.65	0.69	0.54	0.58	0.65
Cr_2O_3	0.09	nd	0.02	nd	0.03
FeO	15.1	14.9	17.2	16.7	16.4
MnO	1.83	1.93	2.23	2.33	2.34
MgO	10.8	11.2	9.6	9.6	11.0
CaO	17.9	17.8	18.0	17.7	17.0
Na_2O	0.65	0.64	0.66	0.69	0.62
TOTAL WT. %	98.6	98.6	99.3	98.3	98.8

Average Weight Percent (All Analyses)

	Average	Range	Nomenclature:
SiO_2	50.4	(50.1-50.9)	c = core analysis
TiO_2	0.66	(0.61-0.72)	e = edge analysis
Al_2O_3	0.62	(0.54-0.69)	nd = not detected
Cr_2O_3	0.03	(0.0-0.09)	
FeO	16.1	(14.9-17.2)	
MnO	2.13	(1.83-2.34)	
MgO	10.4	(9.6-11.2)	
CaO	17.6	(17.0-18.0)	
Na_2O	0.65	(0.62-0.69)	
TOTAL	98.6		

Table 7. Microprobe Analyses of Biotites and Amphiboles, Samples RMD-7, RMD-9, and RMD-10

	Sample				
	RMD-7	RMD-10	RMD-7	RMD-7	RMD-9
	Biotite Phase		Amphibole Phase		
Analysis:	1	2	1	2	3
Crystal ID:	7-B-2a	10-B-2a	7-A-1a	7-A-1b	9-A-2a
Oxide					
SiO_2	32.1	33.5	49.8	51.4	51.7
TiO_2	na	2.26	na	na	1.59
Al_2O_3	14.8	13.6	0.23	0.27	0.37
FeO	25.6	20.0	36.2	25.7	24.7
MnO	na	2.34	na	na	4.46
MgO	10.9	10.6	0.41	0.10	0.07
CaO	0.09	0.06	1.69	7.0	8.4
Na_2O	0.60	1.84	7.4	9.4	6.0
K_2O	7.3	8.5	1.10	0.13	0.08
TOTAL WT. %	91.4	92.7	96.8	94.0	97.4

na = not analyzed during microanalysis

Table 8. Microprobe Analyses of Opaques

	Sample								
	RMD-6			RMD-7				RMD-9	RM-P1-30.0
Analysis:	1	2	3	1	2	3	4	1	1
Crystal ID:	O-1a	O-2b	O-3b	O-2a	O-3a	O-4a	O-6b	O-3a	O-3
Oxide									
TiO_2	20.4	48.1	21.0	1.25	22.0	20.9	49.7	24.2	46.7
Al_2O_3	1.58	0.14	1.57	0.42	1.31	1.82	0.04	1.42	0.13
Cr_2O_3	0.01	nd	nd	0.12	nd	0.01	nd	nd	nd
FeO	72.3	48.8	72.1	87.1	72.2	73.3	43.4	71.3	47.2
MnO	2.34	2.31	2.25	0.03	2.29	1.97	4.10	2.33	2.45
MgO	1.22	0.02	1.41	nd	0.70	0.53	nd	0.78	2.28
TOTAL WT. %	97.9	99.4	98.3	88.9	98.5	98.5	97.2	100.0	98.8
Phase	Ti-Mt	Ilm	Ti-Mt	Hem	Ti-Mt	Ti-Mt (Mn-rich)	Ilm	Ti-Mt	Ilm

Ti-Mt = Titaniferous Magnetite
Ilm = Ilmenite
Hem = Hematite
nd = Not detected in analysis

Table 9. Microprobe Analyses of Glasses and Associated Materials, Samples RMD-1 and RM-P1-53.8

	Sample																	
	RMD-1													RM-P1-53.8				
Analysis:	1	2	3	4	5	6	7	8	9	10	11	12	13	14	15	16	17	18
Point ID:	G-1a	G-2a	G-3a	G-4a	G-5a	G-6a	G-8a	G-11a	G-12a	G-13a	G-1b	G-2b	G-3b	G-3	G-4	G-5	G-7	G-9
Oxide																		
SiO_2	70.3	63.3	70.2	69.4	70.9	69.2	71.6	78.5	71.9	78.3	76.5	76.1	72.9	75.1	76.3	72.2	72.7	76.7
Al_2O_3	13.7	13.5	14.0	13.7	14.2	13.3	13.6	11.5	12.7	10.8	11.6	12.2	11.0	9.1	9.2	11.3	11.6	10.6
FeO	0.22	3.45	0.21	0.22	0.83	0.09	0.19	2.64	3.60	2.18	3.19	2.94	4.60	1.19	0.16	0.06	0.07	0.12
MgO	0.45	0.50	0.47	0.45	0.47	0.48	0.48	nd	nd	nd	nd	nd	nd	nd	0.01	nd	nd	0.08
CaO	2.35	2.15	2.36	2.34	2.20	1.86	1.89	nd	0.02	nd	0.11	0.06	0.31	1.98	1.73	2.44	2.53	1.63
Na_2O	0.75	0.51	0.61	0.82	0.56	0.73	0.93	3.66	5.24	4.37	5.25	4.51	4.64	0.60	0.61	1.03	1.17	0.60
K_2O	3.49	3.08	3.38	3.59	3.47	3.76	3.98	3.82	5.51	4.24	3.30	4.78	4.22	1.10	1.53	1.72	1.74	2.61
TOTAL WT %	91.3	86.5	91.2	90.5	92.4	89.4	92.7	100.1	99.0	99.9	100.0	100.6	97.7	89.1	89.5	88.8	89.8	92.3

Average Weight Percent (Analyses 1-5, 8-13)

Oxide	1-5	Range (1-5)	8-13	Range (8-13)
SiO_2	68.8	(63.3-70.94)	75.7	(71.9-78.5)
Al_2O_3	13.8	(13.7-14.2)	11.6	(10.8-12.7)
FeO	0.95	(0.21-3.45)	3.19	(2.18-4.60)
MgO	0.47	(0.45-0.50)	–	–
CaO	2.27	(2.15-2.36)	0.13	(0.02-0.31)
Na_2O	0.65	(0.51-0.82)	4.61	(3.66-5.24)
K_2O	3.76	(3.08-3.59)	4.31	(3.30-5.51)
TOTAL	90.7		99.5	

nd = not detected in analysis

Feldspars analyzed (Tables 5a to 5i) include both phenocrysts and crystals occurring within pumice clasts and rock fragments. Feldspar phenocrysts are all anorthoclase, a high-temperature, sodium-potassium feldspar restricted in occurrence to felsic volcanic rocks. The presence of anorthoclase phenocrysts without coexisting plagioclase phenocrysts is typical of peralkaline rhyolites. Analyses of phenocryst cores average $An_{4.5}Ab_{56.2}Or_{39.3}$ for all samples; phenocryst edges average $An_{6.1}Ab_{55.8}Or_{38.1}$. Figure 10 shows the restricted range of compositions. K_2O and Na_2O variations between phenocryst edges and cores tend to be irregular. Several phenocryst samples show an increase in CaO from core to edge. These phenocrysts (Figure 11), however, tend to be within more poorly welded samples, where crystallization is extensive or alteration has occurred.

Resorption of feldspar phenocrysts, sometimes noted here, suggests a late-stage increase in H_2O pressure before eruption, resulting in partial melting because of the related decrease in liquidus temperature. The compositions of partially resorbed feldspar phenocrysts in analyzed samples generally overlap those of unresorbed phenocrysts, though there is a slight tendency for Na_2O:K_2O to be higher in partially resorbed crystals (Figure 12). The resorbed phenocrysts may in part be xenocrysts but may also represent early crystallized sodium-rich feldspar. Late-stage disequilibrium with the sodium-depleted residual liquid may be responsible for the preferential resorption of these phenocrysts over more potassic phenocrysts closer to the liquid in composition. This compositional evolution suggests that feldspar fractionation occurred in the magma, as proposed by Noble.[6]

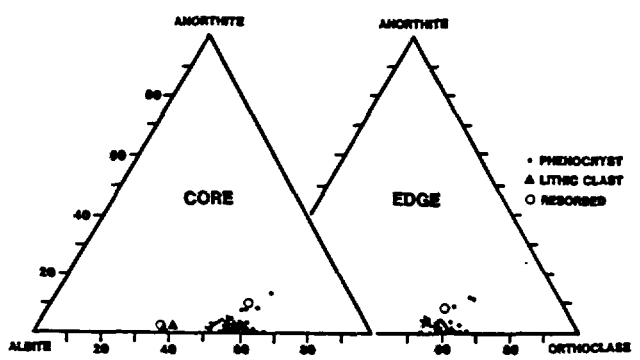

Figure 10. Compositions of Feldspar Phenocrysts From Rocks of the Grouse Canyon Member, as Determined by Electron Microprobe Techniques (Compositions expressed in mole percent end members Albite ($NaAlSi_3O_8$), Anorthite ($CaAl_2Si_2O_8$), and Orthoclase ($KAlSi_3O_8$)

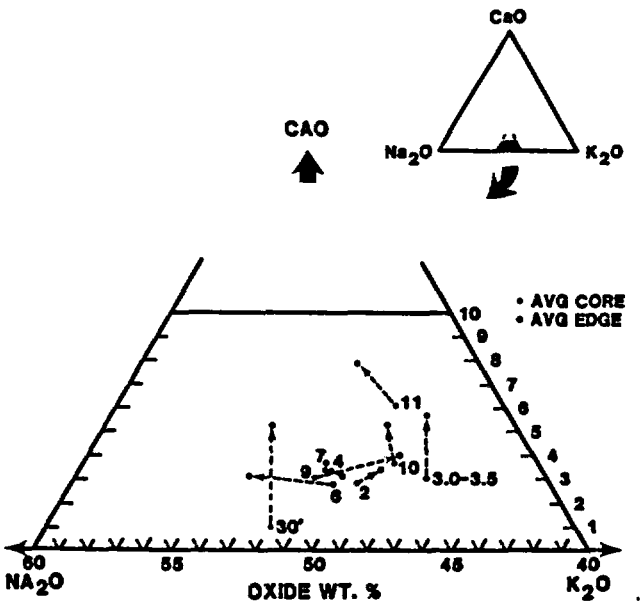

Figure 11. Core-Edge Compositional Zoning of Feldspar Phenocrysts From Rocks of the Grouse Canyon Member, as Determined by Electron Microprobe Techniques

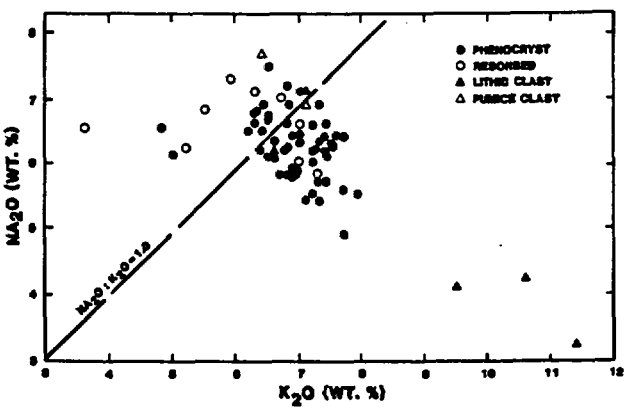

Figure 12. Plot of Na_2O vs K_2O of Feldspar Phenocrysts From Rocks of the Grouse Canyon Member, as Determined by Electron Microprobe Techniques

Feldspars within pumice clasts (Table 5) have compositions similar to those of average phenocrysts, which suggests that the pumice is autolithic. The Transition Zone (RMD-11, Table 5g) contains feldspars that tend to be slightly higher in CaO than do other analyzed anorthoclases in the Grouse Canyon Member, as well as several phenocrysts or xenocrysts of potassium feldspar and plagioclase. This supports petrographic data suggesting that this tuff is not genetically related to the Grouse Canyon Member.

Pyroxenes were analyzed from Unit A (RMD-2) and from the upper part of Unit B (RMD-9) (Table 6). All analyzed grains are small (<0.1 mm) and anhedral; no large phenocrysts were identified in the probe sections. Analyzed pyroxenes are manganiferous, containing an average of 2.13 wt.% MnO; they would be classed as augites or ferroaugites (Figure 13), containing an average of 16.1 wt.% FeO. According to Noble,[8] such iron-rich pyroxene is a common phenocryst phase in silicic peralkaline tuffs. A single sodic pyroxene in the groundmass of Sample RMD-2, apparently an in situ devitrification product, was also analyzed (qualitative analysis not included in Table 6). The abundances of iron, sodium, and silica in the analysis suggest that the phase is aegirine.

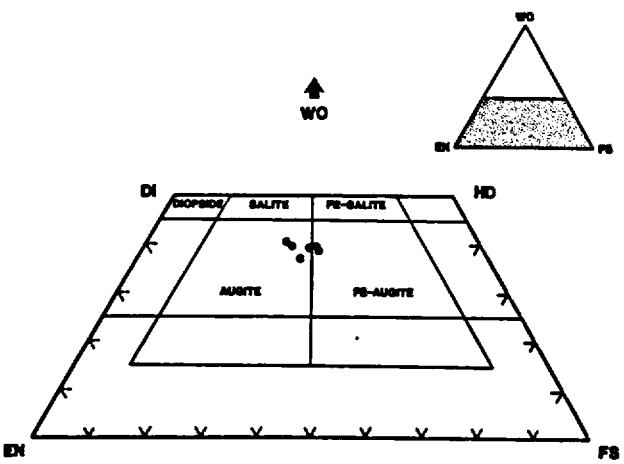

Figure 13. Compositions of Pyroxenes From Rocks of the Grouse Canyon Member, as Determined by Electron Microprobe Techniques (Compositions expressed in mole percent end members, Enstatite (En; $MgSiO_3$), Ferrosilite (Fs; $FeSiO_3$), and Wollastonite (Wo; $CaSiO_3$). Di is Diopside ($Mg_{0.5}Ca_{0.5}SiO_3$) and Hd is Hedenbergite ($Fe_{0.5}Ca_{0.5}SiO_3$).)

Small biotite grains are present in several samples, particularly in the upper part of the Grouse Canyon Member. Many are too small for accurate analysis; all are high in TiO_2. Two representative analyses are included in Table 7.

Amphiboles occur as small needles, usually concentrated near the center of flattened, devitrified pumice fragments. They are common throughout Units B and C but are generally too small for analysis. Analyzed samples (Table 7) are probably iron-rich richterite or arfvedsonite. The amphiboles are invariably associated with axiolitic and spherulitic intergrowths of alkali feldspar and quartz, which suggests they originated during high-temperature devitrification, but after welding.

Various oxide phases are present in grains coarse enough to be analyzed, in addition to the very fine-grained disseminated hematite noted in parts of Unit B. Analyzed opaques include ilmenite, titaniferous magnetite, and manganese oxides (Table 8). Ilmenites are commonly skeletal to lath-shaped; titaniferous magnetites are commonly subhedral to anhedral and variably altered to hematite and limonite. The iron-titanium oxides commonly contain significant amounts of MnO (up to 4% or more).

Manganese oxides, for which no analyses are given here, pervade most samples collected. They occur rarely as anastamosing dendrites, more commonly as amorphous, interstitial material apparently associated with alteration of glass, feldspar, and other oxides. Low analytical totals suggest that the manganese oxides are poorly crystalline and hydrous.

Glass analyses from Tunnel Bed 5 (RMD-1 and RM-P1-53.8, Table 9) generally show low analytical totals, caused largely by hydration and zeolitization. Several glass "blebs" within RMD-1, however, show analytical totals near 100% and are apparently nonhydrated (Table 9, Analyses 8-13). Hydrated and nonhydrated glasses from Tunnel Bed 5 contain distinctly different proportions of several oxides, most notably Al_2O_3, CaO, Na_2O, and K_2O; Al_2O_3 and CaO are enriched in the hydrated glass, Na_2O and K_2O in the nonhydrated glass. FeO contents vary widely but are generally higher in the anhydrous glass. The anhydrous glasses are quite similar in composition to primary glasses from the lowermost Grouse Canyon Member reported by Noble (Table 1, Analyses 1, 3-5), supporting the interpretation that Tunnel Bed 5 in G-Tunnel is correlative with the lower part of the Grouse Canyon Member as mapped on the surface at Rainier Mesa.[12]

Matrix materials analyzed from the Grouse Canyon Member proper in the RMD (Table 10) include optically isotropic glass (G), partially devitrified glass (D), coarsely devitrified pumice and shards (C), and spherulitic to axiolitic crystalline material (Z). Much of the isotropic glass is found rimming resorbed or altered phenocrysts (Table 10, Analyses 6 and 12) or lining pores or bubbles (Table 10, Analyses 21, 23, and 24). Other examples occur throughout the matrix. Judging from their high Al_2O_3, low SiO_2, and high K_2O contents (Analyses 6, 7, 12-14, 21, 22, and 25-29), many of these isotropic glasses appear not to be primary, but may have formed by partial melting of phenocrysts in the magma chamber or after emplacement. Glass analyses 23 and 24 have SiO_2, Al_2O_3, and K_2O values near the assumed primary composition (Table 1, Analyses 1, 3, 4, 5; Table 9, Analyses 10-13) but are apparently enriched in K_2O.

Table 10. Microprobe Analyses of Glasses and Related Materials, Grouse Canyon Member

Sample:	RMD-2				RMD-4		
Analysis:	1	2	3	4	5	6	7
Point ID:	Z-1a	Z-2a	Z-3a	D-1a	Z-1a	G-1a	G-11a
Oxide							
SiO_2	69.4	70.1	79.4	77.34	83.5	67.01	68.3
TiO_2	na	na	na	na	na	na	na
Al_2O_3	13.2	12.7	5.42	11.14	10.12	15.6	14.0
FeO	1.88	1.87	1.20	1.24	0.61	2.71	3.54
MnO	na	na	na	na	na	na	na
MgO	nd	nd	nd	nd	nd	0.36	0.04
CaO	0.04	0.08	0.04	0.01	0.12	0.16	nd
Na_2O	7.0	8.3	6.5	7.5	4.86	4.68	5.51
K_2O	5.69	1.61	4.85	1.54	1.97	8.1	6.8
TOTAL WT %	97.2	94.7	97.4	98.8	101.2	98.6	98.2

Sample:	RMD-4b				RMD-6						
Analysis:	8	9	10	11	12	13	14	15	16	17	18
Point ID:	*	*	*	*	G-1a	G-2a	G-3a	C-1a	C-2a	C-3a	C-1b
Oxide											
SiO_2	68.1	66.1	66.4	75.1	70.4	69.1	69.7	74.6	66.2	75.4	75.6
TiO_2	0.16	0.24	0.29	0.14	na	na	na	na	na	na	na
Al_2O_3	15.7	14.8	15.2	11.1	18.1	15.2	14.4	11.3	15.4	10.8	11.5
FeO	2.41	3.16	5.29	2.64	0.81	2.70	3.55	3.49	3.13	3.25	3.58
MnO	nd	0.97	0.13	0.39	na	na	na	na	na	na	na
MgO	nd	nd	0.03	nd	nd	0.02	nd	0.05	0.03	0.02	nd
CaO	0.01	0.06	0.19	nd	0.09	0.05	0.13	0.06	0.09	0.07	0.16
Na_2O	6.6	6.3	6.4	5.49	7.0	4.33	4.46	5.02	4.83	4.87	5.19
K_2O	7.9	8.3	7.2	5.77	5.67	8.9	9.3	5.43	8.2	4.63	5.10
TOTAL WT %	100.9	99.9	101.1	100.6	102.1	100.3	101.5	100.0	97.9	99.0	101.1

Table 10. (cont)

Sample:	RMD-7			RMD-9			RMD-10		RM-P1-30.0		
Analysis:	19	20	21	22	23	24	25	26	27	28	29
Point ID:	C-1a		G-2	D-1a	G-1b	G-2b	G-1a	G-2a	G-2a	G-3a	G-3b
Oxide	c	e									
SiO_2	77.6	64.0	66.5	65.9	76.5	77.5	67.1	65.9	67.6	68.5	67.7
TiO_2	na	na	na	0.18	0.09	0.03	0.47	na	na	na	na
Al_2O_3	10.8	15.3	15.5	15.0	11.7	10.3	16.0	15.8	14.8	15.0	15.7
FeO	2.01	3.23	3.36	2.99	2.10	2.50	2.92	2.82	2.97	2.40	2.65
MnO	na	na	na	0.05	nd	0.11	0.19	na	na	na	na
MgO	0.02	0.01	0.26	nd	0.06	nd	0.74	0.12	nd	nd	nd
CaO	0.01	0.02	0.41	0.12	0.03	0.05	0.12	0.24	0.08	0.01	0.02
Na_2O	4.52	5.10	6.5	4.56	3.78	4.57	5.61	5.20	3.12	3.61	3.26
K_2O	5.14	8.4	6.7	8.0	6.3	5.19	7.6	7.1	9.4	8.5	9.4
TOTAL WT %	100.1	96.1	99.2	96.8	100.6	100.3	100.8	97.2	98.0	98.0	98.7

Glass (G)
Partially Devitrified Glass (D)
Coarse-Devitrified Pumice and Shards (C)
Spherulite (Z) and Pumice Analyses

c = core analysis
e = edge analysis
na = not analyzed
nd = not detected

*Analyses 8-11 are from a traverse of a devitrified pumice fragment. Analysis 8 is at edge; Analysis 11 at core of fragment.

Coarsely devitrified glass shards and pumice, commonly with spherulitic and axiolitic textures, are present in most welded samples. Because individual crystals are very small, analyses are variable (Table 10, Analyses 15-20). In general, the high SiO_2, Al_2O_3, K_2O, and Na_2O contents shown in these analyses are compatible with petrographic observations that most devitrified material is intergrown quartz/cristobalite and alkali feldspar.

A broad-beam analytical traverse across various optical zones in a flattened and devitrified pumice fragment from the lower part of Unit B (Table 10, Analyses 8-11) appears to indicate that some small-scale elemental migration occurred before or during devitrification. Na_2O and K_2O are enriched on the edges relative to the center, and K_2O:Na_2O is higher. SiO_2 is depleted in material away from the core as in most analyses of altered glass; FeO appears enriched in an intermediate zone. Al_2O_2 is enriched in the silica-depleted zones relative to analyses of unaltered glass. Coarse quartz and alkali feldspar intergrowths and small arfvedsonite laths within vesicular centers of larger pumice fragments also attest to the mobility of elements during devitrification and crystallization. Together, these lines of evidence reflect the existence of only very small domains of chemical equilibrium in the Grouse Canyon Member.

As noted above, whole-rock compositions presented here (Table 2) are slightly higher in total Fe and CaO and lower in K_2O and Na_2O than are average compositions of anhydrous glasses that are thought to be primary (Table 9, Analyses 8-13). Most of this variation (except in the altered and phenocryst-poor RMD-2) can be explained by the presence of alkali feldspar, clinopyroxene, and iron oxide as phenocrysts. Average Na_2O/K_2O is lower in both glasses and whole-rocks analyzed here (1.07 and 0.72, respectively) than in analyses reported by Noble[6] for fresh glassy samples of Grouse Canyon Member (Table 1, Analyses 1, 3-5, average Na_2O/K_2O = 1.20). This suggests that some sodium loss has occurred even in glassy portions of samples from the RMD.

Survey of Clays and Zeolites

Clays and zeolites were identified in several samples by x-ray powder diffraction (XRD) with an automated diffractometer. For these analyses, the clay-sized fraction was separated for analysis by standard procedures outlined by Carroll.[13] The clay-sized fraction was spread evenly on a microscope slide for

analysis and allowed to dry. X-ray diffraction patterns were obtained using nickel-filtered copper k_α radiation. X-ray peaks (degrees 2θ) were recorded by using an automated goniometer and strip chart recorder. Samples were then glycolated and rerun to determine variation in d-spacing with glycolation. Clay mineral identification followed procedures outlined by Carroll[13]; zeolites were identified by comparison with diffractometer patterns presented by Sheppard and Gude.[14]

Table 11 summarizes the clay minerals and zeolites identified and briefly describes sample settings and locations (detailed results are given in Appendix C). Most samples were collected from Unit C in the RMA, in which clay-rich pods and lenses up to 5 cm in length are common. One sample (RMD-3) is altered tuffaceous matrix from the rubble flow zone between Units A and B. Two other samples are clearly associated with tectonic structures: RMD-5 is from a clay pod adjacent to a fracture in Unit B; RMD-16 is from a thin clay seam within a brecciated fault zone in Unit C. LA-1 and LA-2 are from a similar but thicker clay seam in a fault in the Laser Alcove northeast of the RMD.

Table 11. Summary of Identified Clays and Zeolites

Sample	Minerals Identified	Location
RMD-3	Clay fract.: saponite (smectite), mixed layer illite-smectite Silt fract.: illite/ smectite	17.5 ft P, 2.5 ft V; from matrix in rubble flow zone between Units A and B.
RMD-5	Smectite and/or swelling chlorite	40.5 ft P, 5.7 ft V; from ovoid baseball-sized pod of greenish clay with reddish-brown lithic fragments; adj to curved fracture.
RMD-12	Saponite and swelling chlorite	In RM Alcove, left rib, 3 ft from RMD, 8 ft from floor. Mixture of greenish-yellow and dark greenish-gray clay in 1 by 10 cm seam parallel to layering.
RMD-13	White material: smectite Red material: saponite and smectite	In RM Alcove, left rib, 5 ft from RMD, 6 ft from floor. ~3 by 2 cm ovoid pod of white material surrounded by reddish-brown material.
RMD-14	Clay fract.: saponite and mixed layer illite-smectite Silt fract.: saponite	From working face of RM Alcove (on 11/7/80), 4 ft from floor, 2 ft from left rib. ~5-cm-dia reddish-brown clay pod.
RMD-15	Clay fract.: swelling chlorite	From working face of RM Alcove (on 11/7/80), 4 ft from floor, 5.5 ft from left rib, 6 ft below base of Trans Zone. Dark yellowish-green clay with dark splotches in pod ~1.5 by 5 by 10 cm flattened parallel to layering.
RMD-16	Clay fract.: smectite and saponite Silt fract.: smectite, saponite and clinoptilolite	On right rib of RM Alcove, 5.5 ft below base of Trans Zone. Mixture of brownish silt and darker gray clay occurring as a clayey seam within a brecciated fault zone striking ~N80W.
LA-1 & LA-2	Saponite and smectite	From Laser Alcove. From 10-cm-wide clay-silt seam in fault zone similar to that containing sample RMD-16.

Note: Unless otherwise stated, all locations measured from intersection of left rib of RMD and EV6 Incline parallel to floor (P) and vertically up from floor (V)

Clays identified in the samples include smectites, mixed-layer illite/smectite, mixed-layer chlorite/smectite, and swelling chlorite. The XRD patterns of the clay minerals exhibit broad, diffuse peaks, indicating poor crystallinity. The additional analytical procedures needed to identify specific smectite minerals were not applied because of the apparent poor crystallinity of these minerals. There is no correlation between sample location or geologic setting and clay mineral species present.

The zeolite clinoptilolite, in addition to smectite and saponite, was identified in the silt-sized fraction of RMD-16, taken from the fault zone near the end of the RMD. No other zeolites were identified in clay or silt size fractions of any other samples. However, zeolites would probably not be detectable by the analytical method used if they occurred in amounts <20%.

Scanning-Electron-Microscope (SEM) Reconnaissance of Porosity and Zeolites

An SEM equipped with an energy-dispersive x-ray analyzer was used to examine the characteristics of various types of porosity in the RMD samples. This information is important in understanding both the dehydration response of a rock mass on heating[15] and mechanisms and rates of chemical migration through the rock.[16] Though nuclide-migration experiments are not planned in the welded Grouse Canyon Member in G-Tunnel, the survey of characteristics here indicates possible complex porosity in devitrified welded tuffs as a whole. Three distinct types of porosity appear to contribute to the bulk porosity of the rocks: (1) matrix or intergranular porosity; (2) gas bubbles or small vugs; and (3) pores in pumice fragments.

A series of SEM photographs at 1000X magnification were taken to show an area of typical matrix in each of the rocks. Tunnel Bed 5 (RMD-1, Figure 14) has high matrix porosity, primarily the result of loose packing of constituent grains. Unit A of the Grouse Canyon Member (RMD-2, Figure 15) is densely welded and has low matrix porosity. A bulk-property sample from this zone has a calculated total porosity of 0.17 to 0.18.[17] The lower part of Unit B (RMD-4, Figure 16) is less porous than Tunnel Bed 5 but slightly more porous than the more densely welded Unit A. The densely welded middle part of Unit B (RMD-6, Figure 17) has small grain size relative to Units A and C and many small pores in the matrix. Calculated bulk porosity in this zone is 0.12 to 0.16. Matrix porosity in Unit C (RMD-10, Figure 18) is similar to that in the lower part of Unit B, while bulk porosity is 0.20 to 0.28, probably because of extensive vuggy porosity. The sample from the Transition Zone (RMD-11, Figure 19) has matrix porosity higher than the moderately welded parts of the Grouse Canyon Member (e.g., Figure 16), and a calculated total porosity of 0.33.[17]

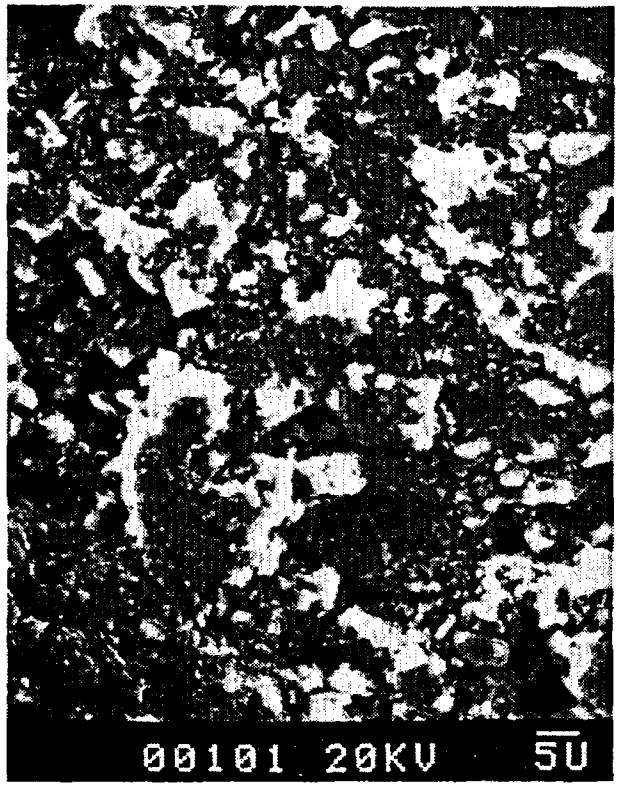

Figure 14. SEM Photograph of Matrix in Sample RMD-1 From Tunnel Bed 5 (5 to 10 μm tabular clinoptilolite crystals are present in pores. Scale bar is 5 μm.)

Figure 15. SEM Photograph of Matrix in Sample RMD-2 of Unit A (Scale bar is 5 μm.)

Figure 16. SEM Photograph of Matrix in Sample RMD-4 of Lower Part of Unit B (Scale bar is 5 μm.)

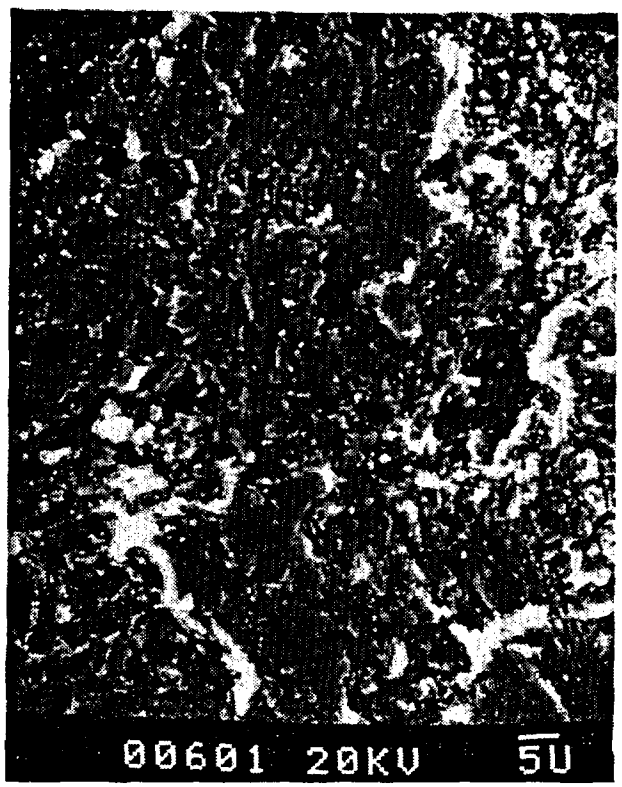

Figure 17. SEM Photograph of Matrix in Sample RMD-6 of Unit C (Scale bar is 5 μm.)

Figure 18. SEM Photograph of Matrix in Sample RMD-10 of Unit C (Scale bar is 5 μm.)

Figure 19. SEM Photograph of Matrix in Sample RMD-11 of Transition Zone (Scale bar is 5 μm.)

Vuggy porosity is most common in the upper part of the Grouse Canyon Member (Unit C); vugs are commonly 0.5 mm or less in diameter and contain vapor-phase-deposited quartz and alkali feldspar (Figure 20). Vugs are rare in the more densely welded, devitrified samples from Units A, B, and C, as well as in samples containing a high percentage of glass. The abundance of vugs in the upper part of the Grouse Canyon Member suggests an upward transport of gases (vapor-phase activity) as the unit cooled.

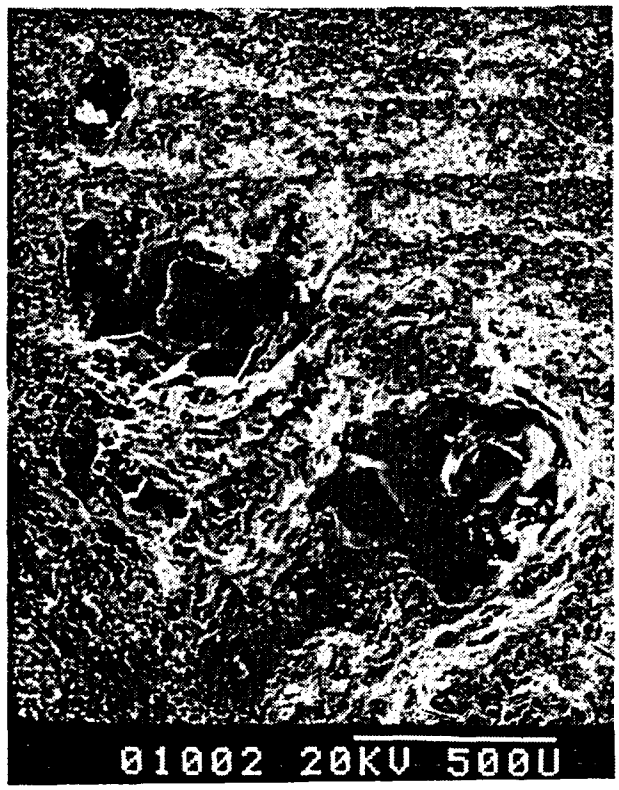

Figure 20. SEM Photograph of Vuggy Pores in Sample RMD-10 of Unit C (Note vapor-phase quartz in pore. Scale bar is 500 μm.)

Pumice pores (Figure 21) are common in poorly welded tuffs within Unit C but are increasingly flattened and destroyed in more densely welded, recrystallized zones. Pumice porosity is probably a large percentage of the total porosity in less densely welded tuffs.

The zeolite clinoptilolite was tentatively identified in pores in hydrated pumice within the uppermost portion of Tunnel Bed 5 (Figure 22). Reliable energy dispersive analyses could not be obtained, however, because of the very small size of the crystals (<5 μm) and the restriction of crystals to pores. Work in progress on Tunnel Bed 5 indicates that zeolitization is very extensive throughout most of the unit.

Figure 21. SEM Photograph of Pores in Slightly Flattened Pumice in Sample RMD-10 of Unit C (Scale bar is 500 μm.)

Figure 22. SEM Photograph of Clinoptilolite Crystals in Pore Within Pumice Fragment in Sample RMD-1 of Tunnel Bed 5 (Scale bar is 5 μm.)

Summary and Comparison of the Grouse Canyon and Topopah Spring Members

The detailed results of this study are summarized in the left-hand columns of Table 12 and are therefore not repeated here. The right-hand column of Table 12 lists comparable characteristics of the Topopah Spring Member. The most fundamental difference between the two units is bulk composition; the Grouse Canyon Member is marginally peralkaline; the Topopah Spring Member is subalkaline. This difference in bulk composition appears to have had little effect on the major mineralogical makeup of the two units since both units consist largely of feldspar and a silica polymorph. However, bulk composition appears to have had major impact on welding, porosity, devitrification, silica-polymorph mineralogy, and composition of accessory silicate phases.

Lipman[23] estimates that opaques in the Topopah Spring Member crystallized at temperatures ranging from ~700°C in the lower rhyolitic portion of the unit to as much as 900°C for the upper caprock, which is quartz latitic in composition. No such detailed study has been carried out in the Grouse Canyon Member. However, Schmincke[24] concludes that peralkaline tuffs in general are erupted at higher temperatures and have lower initial volatile contents and viscosities than analogous calc-alkaline tuffs. As a result of the higher initial temperatures and lower viscosities, dense welding is common even in relatively thin peralkaline tuffs,[24] as has been noted previously in the Grouse Canyon Member.[5] Higher emplacement temperatures also appear to account for the domination of quartz over cristobalite or tridymite in devitrified portions of perkaline tuffs, such as the Grouse Canyon Member.[5,24] Rapid cooling, a result of the relative thinness of the unit, appears to account for the strong fracturing of the Grouse Canyon Member. Thus, the major consequence of the initial perkaline composition of the Grouse Canyon Member is that, although thin, this unit is moderately to densely welded, largely devitrified to quartz and feldspars, and intensely fractured. It is thus more similar to thick devitrified portions of the Topopah Spring Member than would be expected of a calc-alkaline flow only 14 m thick.

There are, however, other consequences of the peralkaline composition of the Grouse Canyon Member. First, the presence of excess alkalis has resulted in formation of minor amounts of sodic amphiboles and pyroxenes, phases not found in the Topopah Spring Member. The mode of occurrence of these minerals indicates that they are high-temperature phases, resulting directly from devitrification. Their low abundance and probable thermal stability indicate that they would have no impact on thermomechanical response of the rock mass. Because of incomplete devitrification, alkali-rich glass is generally present in small amounts in the matrix of the Grouse Canyon Member. However, thermal conductivity and thermal expansion measurements to date[25] indicate that this glass has no measurable impact on expansion or conductivity behavior. No contraction that might be related to dehydration of glass has been noted in thermal expansion measurements, and disagreement between theoretical and measured thermal conductivities is no greater for the Grouse Canyon Member than for other tuffs. In fact, because of the absence of widespread clays, thermal expansion behavior of the Grouse Canyon Member appears to be more uniform than that of the Topopah Spring Member.

Glass in the matrix of the Grouse Canyon Member might well not be stable during long periods of heating if water is present and might either devitrify or react to form secondary phases. Given the relatively small amount of glass, however, no problem appears to exist for thermomechanical experiments, with the possible exception of parts of Unit A. The presence of alkali-rich glass might make detailed interpretation of nuclide-migration experiments in the welded Grouse Canyon Member in G-Tunnel more complex than for a similar experiment run in glass-free parts of the Topopah Spring Member. Whether or not the existence of glass would qualitatively affect the results is not clear; no such experiments are currently planned for G-Tunnel.

The limited thickness of the Grouse Canyon Member suggests that thermomechanical experiments should probably be restricted to Unit B and the lower portions of Unit C, and that no tests larger in general scale than individual simulated waste canisters can be run without encountering boundary or layering effects. The lack of lithophysae in the Grouse Canyon Member indicates that no direct information about the thermomechanical response of lithophysal portions of the Topopah Spring Member can be gained directly from experiments operated in the welded tuffs in G-Tunnel. Comparisons between these Members, and their location at comparable depths in G-Tunnel and at Yucca Mountain above the static water level suggest, however, that thermomechanical experiments in the welded Grouse Canyon Member on a scale no larger than that of individual canisters should be transferable to welded, nonlithophysal portions of the Topopah Spring Member at Yucca Mountain.

Table 12. General Comparison of Grouse Canyon Member, Belted Range Tuff, RMD, With Topopah Spring Member, Paintbrush Tuff, Yucca Mountain*

Factor	Grouse Canyon Member	Topopah Spring Member
I. General Character		
A. Bulk Chemistry	Marginally peralkaline but relatively uniform. $(Na_2O+K_2O)/Al_2O_3$ = 0.95 to 1.007; 71 to 75 wt% SiO_2; Differentiation Index = 96.2 to 93.9, decreasing upwards.	Subalkaline, relatively variable. $(Na_2O+K_2O)/Al_2O_3$ = 0.81 to 0.93; 69 to 77 wt% SiO_2; Differentiation Index = 95.8 to 89.7, decreasing upwards.
B. Total Thickness	~ 14 m.	Variable; published reports indicate that total thickness = 304 to 363 m.
C. Flow Units	Three distinct flow units, separated by distinct but intermittent rubble flow zones.	Six local flow units identified; identification difficult and ongoing, generally by means of lithophysae distributions.
D. Welding (Matrix Porosity)	Bulk of unit moderately to densely welded, general porosity in Unit B = 0.12 to 0.15; moderate breaks in degree of welding across rubble flow zones.	Bulk of unit densely welded; general porosity in lower devitrified portion = 0.08 to 0.16; apparently limited variations in degree of welding across flow and cooling units.
E. Internal Complexity	Minor; major unknown is distribution and continuity of rubble flow zones.	Major; critical unknown is lateral and vertical distribution, properties, and consequences of lithophysal zones.
F. Fracturing	Joints abundant; general spacing <1 m, but variable; small faults and breakage zones evident.	Jointing highly variable, generally intense in densely welded nonlithophysal zones and lithophysal intervals; joint spacing in nonlithophysal zones may be less than in Grouse Canyon Member; faulting not uncommon; 5 and 6 brecciated zones identified in unit in Holes G1 and A1.
G. Depth	~400 m.	Variable; lower devitrified portion generally 300 to 400 m over most of Yucca Mountain, deeper on east side than on west.
H. Overall Setting	200^+ m above static water level (SWL).	Variable; well above SWL in western part of Yucca Mountain, below SWL on eastern side.

*Data for the Grouse Canyon Member are from this report and Ref 5. Data for the Topopah Spring Member are from Refs 18-22.

Table 12. (Cont)

Factor	Grouse Canyon Member	Topopah Spring Member
II. Thickness Available for Thermomechanical Testing	8 to 10 m, from top of rubble flow zone between Units A and B into upper part of Unit C. Available thickness may be locally limited by rubble flow between Units B and C. Entire thickness free of lithophysae.	Highly variable. Thicknesses effectively free of lithophysae (10%) appear to range from 25 to >80 m. Large thickness of lithophysal tuff also available.
III. Mineralogy		
A. Devitrification	Moderate to nearly complete; devitrification appears to increase upwards through unit; $(Na_2O+K_2O)/Al_2O_3$ of relict glasses = 1.06 to 1.22.	Essentially complete, except for upper and lower vitrophyres.
B. Silica Polymorph	Thermal-expansion and bulk-property data indicate cristobalite present only in lower portion of unit.	Thermal-expansion, bulk-property, and mineralogical data indicate cristobalite and quartz both generally present through bulk of unit.
C. Feldspars (Phenocrysts)	Alkali feldspar (anorthoclase) relatively abundant (6% to 10%), $An_{4-6}Ab_{55-56}Or_{39-40}$; plagioclase generally absent, except small amounts in Unit C.	Alkali feldspar relatively uncommon (≤3%), $An_{1-4}Ab_{47-48}Or_{52-58}$. Plagioclase not uncommon, $An_{20-30}Ab_{65-80}Or_{3-10}$.
D. Accessory Silicates	Marginally peralkaline composition results in presence of small amounts of richterite-arfvedsonite (sodic amphibole) and trace of aegirine (sodic pyroxene); fayalite (Fe-olivine) reported from Grouse Canyon Member, but not noted here; small amounts of biotite are present.	Biotite and clinopyroxene, apatite, zircon, brown (oxy?) hornblende, and allanite; the last four phases are present mainly in the caprock.
E. Clay Minerals	Not noted except in Unit C and where alteration is apparently related to structural control; phases identified include smectite, mixed-layer illite/smectite, mixed-layer chlorite/smectite, and swelling chlorite.	Smectite clays minor (generally ≤5%), but widespread through bulk of unit, apparently a result of widespread vapor-phase activity; in places, clays also thought to result directly from devitrification.
F. Opaques	Disseminated hematite widespread in most densely welded portions, giving characteristic reddish color; ilmenite, titaniferous magnetite, and hydrated (?) manganese oxides also present.	Opaque Fe-Ti oxides (ilmenite-magnetite pairs) in densely welded, devitrified portions show extreme oxidation exsolution caused by widespread vapor-phase activity.

References

[1]K. A. Sargent, D. C. Noble, and E. B. Ekren, "Belted Range Tuff of Nye and Lincoln Counties, Nevada," *Changes in Stratigraphic Nomenclature by the US Geological Survey, 1964*, ed G. V. Cohee and M. S. West, *US Geol Surv Bull 1224-A*, pp A32-A36 (Washington, DC: US Geol Survey, 1965).

[2]B. S. Langkopf and E. Eshom, *Site Exploration for Rock-Mechanics Field Tests in the Welded Grouse Canyon Member, Belted Range Tuff, U12g Tunnel Complex, Nevada Test Site*, SAND81-1897 (Albuquerque, NM: Sandia National Laboratories, February 1982).

[3]R. M. Zimmerman, *Test Plan for Rock-Mechanics Field Experiments in Tuff in G-Tunnel, NTS*, SAND82-0108 (Albuquerque, NM: Sandia National Laboratories, to be published).

[4]F. M. Byers, Jr., W. J. Carr, P. P. Orkild, W. D. Quinlivan, and K. A. Sargent, *Volcanic Suites and Related Cauldrons of Timber Mountain - Oasis Valley Caldera Complex, Southern Nevada*, US Geol Survey Prof Paper 919 (Washington, DC: GPO, 1976).

[5]D. C. Noble, K. A. Sargent, H. H. Mehnert, E. B. Ekren, and F. M. Byers, Jr., "Silent Canyon Volcanic Center, Nye County, Nevada," *Nevada Test Site*, ed E. B. Eckel, Geol Soc Am Memoir 110, pp 65-75, 1968.

[6]D. C. Noble, "Loss of Sodium from Crystallized Comendite Welded Tuffs of the Miocene Grouse Canyon Member of the Belted Range Tuff, Nevada," *Geol Soc Am Bull*, 81:2677-2688, 1970.

[7]B. M. Crowe and K. A. Sargent, *Major-Element Geochemistry of the Silent Canyon - Black Mountain Peralkaline Volcanic Centers, Northwestern Nevada Test Site - Applications to Assessment of Renewed Volcanism*, US Geol Survey Open-File Rpt 79-926 (Washington, DC: US Geol Survey, 1979).

[8]D. C. Noble, "Systematic Variation of Major Elements in Comendite and Pantellerite Glasses," *Earth and Planetary Sci Letters*, 4:167-172, 1968.

[9]D. C. Noble, J. Haffty, and C. E. Hedge, "Strontium and Magnesium Contents of Some Natural Peralkaline Silicic Glasses and Their Petrogenetic Significance," *Am J Sci*, 267:598-608, 1969.

[10]R. L. Smith, *Zones and Zonal Variations in Welded Ash Flows*, US Geol Survey Prof Paper 354-F, pp 149-159 (Washington, DC: GPO, 1960).

[11]A. E. Bence and A. L. Albee, "Empirical Correction Factors for the Electron Microanalysis of Silicates and Oxides," *J Geol*, 76:382-403, 1968.

[12]A. B. Gibbons, E. N. Hinrichs, W. B. Hansen, and R. W. Lemke, "Geology of the Rainier Mesa Quadrangle, Nye County, Nevada," US Geol Survey Geol Quad Map GQ-215 (Washington, DC: US Geol Survey, 1963).

[13]D. Carroll, *Clay Minerals: A Guide to Their X-Ray Identification*, Geol Soc Am Special Paper 126 (Boulder, CO: Geol Soc Am, 1969).

[14]R. A. Sheppard and A. J. Gude III, *Diagenesis of Tuffs in the Barstow Formation, Mud Hills, San Bernardino County, California*, US Geol Survey Prof Paper 126 (Washington, DC: GPO, 1969).

[15]J. K. Johnstone, G. R. Hadley, and D. R. Waymire, *In Situ Tuff Water Migration/Heater Experiment: Final Report*, SAND81-1918 (Albuquerque, NM: Sandia National Laboratories, to be published).

[16]K. L. Erickson and D. R. Fortney, *Preliminary Transport Analysis for Design of the Tuff Radionuclide Migration Field Experiments*, SAND81-1253 (Albuquerque, NM: Sandia National Laboratories, September 1981).

[17]Memorandum from B. S. Langkopf, Sandia National Laboratories, to Distribution, "Bulk Property Measurements in Rock-Mechanics Drift/G-Tunnel," January 30, 1981.

[18]P. W. Lipman, R. L. Christiansen, and J. T. O'Connor, *A Compositionally Zoned Ash-Flow Sheet in Southern Nevada*, US Geol Survey Prof Paper 524-F (Washington, DC: GPO, 1966).

[19]P. R. Carroll and A. C. Waters, ed, *Preliminary Stratigraphic and Petrologic Characterization of Core Samples from USW-G1, Yucca Mountain, Nevada*, LA-8840-MS (Los Alamos, NM: Los Alamos National Laboratories, November 1981).

[20]R. W. Spengler, P. C. Muller, and R. B. Livermore, *Preliminary Report on the Geology and Geophysics of Drill Hole UE25a-1, Yucca Mountain, Nevada Test Site*, US Geol Survey Open-File Rpt 79-1244 (Denver, CO: US Geol Survey, 1979).

[21]M. L. Sykes, G. H. Heiken, and J. R. Smyth, *Mineralogy and Petrology of Tuff Units from the UE25a-1 Drill Site, Yucca Mountain, Nevada*, LA-8139-MS (Los Alamos, NM: Los Alamos National Laboratory, 1979).

[22]P. I. Carroll, F. A. Caporuscio, and D. L. Bish, *Further Description of the Petrology of the Topopah Springs Member of the Paintbrush Tuff in Drill Holes UE25A-1 and USW-G1, and of the Lithic-Rich Tuff in USW-G1, Yucca Mountain, Nevada*, LA-9000-MS (Los Alamos, NM: Los Alamos National Laboratory, 1981).

[23]P. W. Lipman, "Iron-Titanium Oxide Phenocrysts in Compositionally Zoned Ash-Flow Sheets from Southern Nevada," *J Geol*, 79:438-456, 1971.

[24]H. U. Schmincke, "Volcanological Aspects of Peralkaline Silicic Welded Ash-Flow Tuffs," *Bull Volcanologique*, 38:594-636, 1974.

[25]A. R. Lappin, *Thermal and Mechanical Properties of the Welded Grouse Canyon Member and Nonwelded Tunnel Bed 5, G-Tunnel, Nevada Test Site*, SAND82-2203 (Albuquerque, NM: Sandia National Laboratories, in preparation).

APPENDIX A

Analytical Method for Bulk Chemical Analyses

Silica was determined gravimetrically by fusion with sodium carbonate, dehydration with HCl, and weighing as SiO_2. Sulfur was determined on the filtrate by precipitation with $BaCl_2$ and weighing as $BaSO_4$.

Total Fe, Al_2O_3, MgO, CaO, Na_2O, K_2O, TiO_2, MnO, and SrO were determined by atomic absorption spectrophotometry by a method developed by J. Husler at UNM. The Fe, Al, Mg, Ca, Ti, and Sr were determined in an acetylene-N_2O flame after adding Cs to the solutions to minimize ionization interference. The Na, K, and Mn were determined in an acetylene-air flame. Calibration curves were prepared from in-house standards prepared from USGS standard rocks.

The P_2O_5 was determined colorimetrically by an adaptation by J. Husler of the Molybdenum Blue Method, again using rock standards analyzed against USGS standard rocks.

The $H_2O(-)$ was determined by weight loss at 110°C, and the loss on ignition (L.O.I.) was determined by weight loss from 110° to 1000°. The $H_2O(+)$ was estimated by adding to the loss on ignition the weight of oxygen gained by oxidation of FeO to Fe_2O_3. The ferrous iron and the change in weight because of oxidation of ferrous iron were found by determination of the ferrous iron in both the ignited and unignited sample. These were done by H_2SO_4-HF dissolution of the samples followed by titration of Fe^{2+} with standard $K_2Cr_2O_7$ using diphenylamine sulfonic acid sodium salt as an indicator.

APPENDIX B

Descriptions of Individual RMD Samples

Table B1 summarizes modal petrographic data presented in the detailed thin-section descriptions that follow.

Welding terminology used in the descriptions is defined as follows.

- Nonwelded—no in situ deformation of components.
- Slightly welded—minor deformation and obvious preferred orientation of shards in matrix.
- Moderately welded—strong deformation and preferred orientation in shard matrix, with extensive flattening of pumice fragments and some flow deformation in matrix.
- Densely welded—extreme deformation, with extensive flow deformation resulting in strong preferred orientation of shard matrix; extreme flattening of pumice fragments with almost total loss of porosity.

Porosity estimates are based on a count of pores that are easily visible microscopically, generally with pore size >10 microns; large underestimates relative to bulk porosity data are caused primarily by the dominance of submicron-diameter pores, not countable by standard petrographic methods.

Table B2 presents mesoscopic descriptions of fracture filling and clay samples.

Table B3 offers petrographic observations of supplemental sample U12g RM-P1.

Table B1. Modal Analysis Summary for RMD Samples

Constituent	Sample							
	RMD-1 (Tunnel Bed 5)	RMD-2 (Grouse Canyon Unit A)	RMD-4 (Grouse Canyon Unit B)	RMD-6 (Grouse Canyon Unit B)	RMD-7 (Grouse Canyon Unit B)	RMD-9 (Grouse Canyon Unit B)	RMD-10 (Grouse Canyon Unit C)	RMD-11 (Transition Zone)
Textural Makeup:								
Glass shards[1]	5	84	68	62	57	50	56	70
Pumice	70[7]	11	1	12	12	25	6	2
Altered perlite	5[7]							
Rock fragments[2]		2	4	8	15	5	3	3
Phenocrysts:								
Alkali feldspar		2	8	12	12	13	11	8
Quartz				1	1	1	2	
Plagioclase[3]		tr	tr	tr				1
Microcline[3]							tr	
Clinopyroxene		tr	tr	tr		tr		tr
Olivine[3]							tr	tr
Amphibole				tr	tr			
Opaques			1	1	1	1	2	1
Coarse devitrification[4]			17	2			14	
Zeolite and clay	Note[7]	1						tr
Porosity[5]	20		1	2	2	5	6	15
TOTAL	100	100	100	100	100	100	100	100
Estimation Method[6]	E	566	321	409	E	E	385	E

Notes: [1]Increasingly devitrified upward throughout Grouse Canyon Member
[2]Chiefly volcanic; includes some microcrystalline chert and argillite
[3]Highly altered throughout Grouse Canyon Member
[4]Much crystallized in situ from pumice fragments and shard matrix
[5]Only pores >10 to 20 μm included in count
[6]Number of points if by point count; E indicates visual estimate
[7]Largely replaced by zeolites; zeolite abundance in RMD-1 probably >30%
tr = trace

Tuff Thin Section Description: Sample RMD-1

Petrographer: J. R. Connolly

Thin Section Orientation: Approximately perpendicular to layering

Location: Left rib of RMD, 1.5 ft parallel to floor, 1 ft vertical, Tunnel Bed 5

Rock Name: Nonwelded pumice-rich tuff

Constituents: (modes estimated by visual approximation)

Est %	Fragment	Size-Range	Shape	Miscellaneous
5	Glass shards	Generally <0.2 mm	Generally elongate; occasional Y shapes	Original textures largely obscured by alteration
70	Pumice	1 mm uncollapsed, 0.2 to 0.5 mm collapsed	Subround to flattened	Small, white, frothy
5	Altered perlite	1 cm to 1.5 cm	Generally subrounded	Brown bubbles 0.5 to 1 mm diameter, zeolite in pores

Percent Void Space: Estimated ~20%; large margin of error because of plucking. Voids occur as interfragment voids and as bubbles in pumice.

Welding: Slight. Rock contains much pale greenish-brown, frothy pumice with approximately spherical vesicles and a lesser amount of variably collapsed pumice. Glass shard structure is poorly preserved because of devitrification but shows slight preferred orientation suggestive of some welding.

Devitrification: Partial but extensive. Crystals occur as wispy, very fine-grained intergrowths of a clear low-relief, low-birefringence mineral and a pale reddish-brown mineral with higher relief. Crystallization appears to mimic structures of collapsed pumice, though needle-shaped crystallites occur that cut these structures. Devitrification products occur in crystals generally <0.05 mm across. Crystallization has taken place in concentric rings lining bubbles in altered perlite; this may include a considerable amount of zeolite (probably >30%).

Mesoscopic Description: Rock is brown with (1) irregular but generally rod-shaped, dark microcrystalline material, ~1 to 2 mm by 3 to 6 mm, flattened in the plane of foliation (= plane of welding, = bedding); (2) pale brownish-yellow microcrystalline material, slightly flattened parallel to bedding (average 2 mm by 4 mm) that appears to pseudomorph pumice fragments. Dark material may be pseudomorphous after hornblende or pyroxene. Pale brown matrix is microcrystalline. Welding, as indicated by pumice flattening, appears to be very slight. Rock has a very altered overall appearance.

Thin section cut perpendicular to layering; no lineation is evident.

Tuff Thin Section Description: Sample RMD-2

Petrographer: J. R. Connolly

Thin Section Orientation: Approximately perpendicular to layering

Location: Left rib of RMD, 8 ft parallel to floor, 2.5 ft vertical; Grouse Canyon Member

Rock Name: Moderately welded ash-flow tuff – Unit A

Constituents: (modes estimated by 566 point count)

Est %	Fragment	Size-Range	Shape	Miscellaneous
84	Glass shards	Most 0.2 mm Max 1 mm long	Generally elongate; some V & Y shapes	Variably devitrified; 20% of count (17%) is yellow semi-isotropic material
11	Pumice	Max few mm long	Very strongly flattened	Extremely devitrified and difficult to identify positively
2	Anorthoclase	Max 2 to 4 mm	Subhedral, commonly broken	Locally resorbed, enclosing glass or devitrified materials
2	Rock fragments	0.5 to 2.5 mm volcanic largest	Generally subrounded	Volcanic dominant, fine-grained silicious and argillaceous subordinate
<1	Zeolite?	1 to 2 mm aggregates	Generally ovoid	Fills voids locally
Trace	Plagioclase	1 mm or less	Subhedral, broken	Albite twinning
Trace	Clinopyroxene	1 mm or less	Subhedral	Second-order, blue birefringence; extinction angle 45°

Percent Void Space: Not counted but estimated to be <2%

Welding: Moderate to dense; however, original textures are commonly obscured by devitrification. Glass shards show strong elongation and flattening (eutaxitic structure) parallel to foliation, with moderate bowing around competent crystals and rock fragments. Pumice is strongly flattened with void space not obvious; is also largely devitrified.

Devitrification: Moderate; mostly evident on high magnification. Pumice in general is most extensively devitrified to a fine crystal mosaic that obscures pumice texture. Shards locally show axiolitic devitrification.

Fine, crystalline, brownish-yellow material (<0.3 mm) and darker, almost isotropic, brown to opaque material is common (17% to 20%) in shard-rich matrix.

Miscellaneous Textures-Fabric: Crystal resorption is common, and many angular fragments are present.

Some rotational distortion of shards around rounded rock fragments suggests minor postemplacement flowage.

Mesoscopic Description: Rock is pale greenish-brown, apparently thoroughly devitrified but microcrystalline so that it still fractures somewhat concoidally. Devitrified matrix is ~70% of rock. Crystalline fragments include water-clear sanidine (average 1.5 mm by 5 mm), minor quartz, and some dark brown pyroxene(?). Dendritic "splotches" (up to 5 mm across) may be altered mineral phases and are up to 20% of rock on fracture surfaces. Slightly lighter, devitrified fragments, 1 to 6 cm across, are scattered throughout. White to pale buff, ovoid material (zeolite?) is ~1% of mode and is distributed fairly uniformly.

There is no notable preferred orientation of rock fragments or crystals, suggesting a minimal degree of welding. Layering is suggested by crude platy partings.

Tuff Thin Section Description: Sample RMD-4

Petrographer: J. R. Connolly

Thin Section Orientation: Approximately perpendicular to layering

Location: Left rib of RMD, ~34 ft parallel to floor, 2 ft vertical

Rock Name: Slightly to moderately welded ash-flow tuff – Unit B

Constituents: (mode estimates based on 321 point count)

Est %	Fragment	Size-Range	Shape	Miscellaneous
68 (36% optically devitrified, 32% isotropic)	Glass shards	<0.5 mm	Elongate, many Y & V shapes, some bubbles	"Isotropic" glass may be cryptocrystalline
1	Pumice	Average 1 mm	Most undeformed with preserved voids	Some may be devitrified and incl with devitrified minerals below
17	Coarse devitrified products	Fills voids up to several millimetres, and as "fracture filling" that may be replacements of rock or pumice fragments. Includes several distinct crystal types: • Clear with "fan" morphology, sometimes pinkish • Small brownish needles • Brownish-yellow granules		
8	Alkali feldspar	Average 1 to 2 mm, up to 3 mm	Subhedral, broken and/or embayed	Biax(−), 2V 35° to 40°, microperthitic, probably anorthoclase
4	Rock fragments	Generally 1 mm or less	Subrounded	Approximately equal amounts of volcanic and fine-grain clastics, in general extensively recrystallized
1	Opaque	Anhedral irregular patches, brown to black, probably devitrification products		
Trace	Plagioclase, Pyroxene	<0.5 mm	Irregular crystals	

Percent Void Space: 1% counted. Appears minimal, but glass and plucking makes estimate very difficult.

Welding: Slight to moderate. Some extremely devitrified areas may be collapsed pumice fragments, but all pumice recognizable as such is virtually undeformed. Shards, though highly devitrified, are only slightly flattened, and preferred orientation is generally weak; some Y- and V-shaped bubble wall shards are well preserved, and one intact bubble is present.

Devitrification: Extensive; may be almost complete. More than 50% of matrix is coarsely crystalline enough not to be isotropic, and rest may be cryptocrystalline. Devitrification products may locally include some zeolites. Coarse devitrification products (17% of mode) may include devitrified pumice, void fillings, and veinlets but are too coarsely crystalline to allow deduction of original material.

Miscellaneous Textures-Fabric: Lesser degree of welding in comparison with vitric tuff below the rubble flow zone implies that the vitric tuff (Sample RMD-2) was a separate eruptive unit from RMD-4 and has a partially different cooling history than the rest of the Grouse Canyon Member above the rubble flow zone.

Mesoscopic Description: Rock is pale reddish-brown and moderately welded, as indicated by the presence of strongly flattened, partly collapsed pumice lenticles of dark color. Matrix (reddish-brown) is ~60% of rock; crystals are ~6% and include alkali feldspar (average 5 mm by 1.5 mm) with subordinate dark green to black pyroxene(?) and some quartz. Collapsed pumice lenticles are present, and rock is rich in variously altered fragments, mostly volcanic, with some altered, fine-grained sedimentary types.

Pumice fragments are not all dark and strongly flattened, and some contain vapor-phase minerals suggesting nonuniform welding and compaction. This may be a revesiculation associated with gas release during devitrification.

Thin section is not likely to be representative of average composition because of wide variation in lithics and large size of fragments.

Tuff Thin Section Description: Sample RMD-6

Petrographer: J. R. Connolly

Thin Section Orientation: Approximately perpendicular to layering

Location: Left rib of RMD, ~44.5 ft parallel to floor, 6 ft vertical

Rock Name: Densely welded ash-flow tuff – Unit B

Constituents: (mode estimates based on 409 point count)

Est %	Fragment	Size-Range	Shape	Miscellaneous
62 (51% optically devitrified, 11% isotropic)	Glass shards	<0.5 mm	Strongly elongate; rare V & Y shapes	Most recognizable shards show axiolitic devitrification
12*	Pumice	Up to 1 cm long	Strongly flattened; length to 10X width	Most totally devitrified, with loss of porosity
2*	Coarse, devitrified products	Variable size and shape, some pore filling, some vapor phase, some replacing rock fragments		Many include some zeolites as pore filling
12	Alkali feldspar	Range <1 mm to 4 mm	Subhedral, partly resorbed	Vapor-phase minerals in resorbed embayments
1	Quartz	<0.5 mm	Anhedral, irregular to euhedral wedge shape	
8*	Rock fragments	Between 1 mm and 5 mm	Subangular to subrounded	Fine grained subvolcanic and sediments, highly recrystallized
1	Opaque	Poikilitic skeletal zones to 1 mm and smaller granules		Generally brownish, probably hydrated Fe oxides
Trace	Pyroxene, Plagioclase, Amphibole			

*Because of devitrification, coarse devitrification products may in part include some altered rock fragments or pumice.

Percent Void Space: 2% in point count. Voids occur in matrix, within embayed crystals, and rarely in pumice fragments.

Welding: Dense, very strong. Glass shards show extreme distortion and are bent around competent crystal fragments. Pumice fragments are extensively flattened with ragged edges and extensively devitrified, although rare areas (<1%) appear undeformed, with preserved bubbles; this implies nonuniform welding or, perhaps, revesiculation by fluids released during vapor-phase activity. Preferred orientation of shard and pumice long dimensions is very strong.

Devitrification: Extensive. Matrix devitrification products include 5% to 10% Fe_2O_3 (giving overall brick-red color), plus low-relief, clear mineral several tens of microns (alkali feldspar?). "Isotropic" matrix is faintly birefringent on very high magnification (400X) and is probably cryptocrystalline. Coarse crystals (up to 0.1 mm) occur as axiolites replacing pumice; shards include fan-shaped intergrowths of alkali feldspar, cristobalite(?), and small brownish-green pleochroic rods (amphibole?).

Miscellaneous Textures-Fabric: Size sorting of recognizable fragmental material is poor.

Mesoscopic Description: Rock is a brick-red color in matrix with abundant black, collapsed pumice lenticles that have very little relict porosity and are locally a dark, glassy material. Lenticles are commonly surrounded by a reddish rim that is slightly lighter in color than the rock matrix. Some less flattened, brownish frothy zones contain vapor-phase materials and may be vapor-phase cavities. Vapor-phase minerals also line cavities in pumice lenticles and fractures. A few white "granitic" fragments are present. Approximately 8% crystals are present, chiefly alkali feldspar with subordinate biotite(?), pyroxene(?), and quartz.

Tuff Thin Section Description: Sample RMD-7

Petrographer: J. R. Connolly

Thin Section Orientation: Approximately perpendicular to eutaxitic foliation/layering

Location: Left rib of RMD, ~52 ft parallel to floor, 2 ft vertical

Rock Name: Densely to moderately welded ash-flow tuff – Unit B

Constituents: (modes estimated visually because of abundant rock fragments in the slide)

Est %	Fragment	Size-Range	Shape	Miscellaneous
57 (52% optically devitrified, 5% isotropic)	Shards	Most <0.5 mm	Strongly elongate; rare Y & V shapes	Larger shards show axiolitic devitrification
12	Pumice	<2 cm	Strongly flattened	Most extremely devitrified to radiating crystalline aggregates
12	Alkali feldspar	1 to 3 mm	Subhedral	Commonly broken or embayed; devitrified glass in embayments
1	Quartz	<0.5 mm	Irregular to subrounded	Common as small crystals in matrix
15	Rock fragments	1 cm or less	Subrounded	Most "microgranite" – probably recrystallized volcanic, + fine-grain sedimentary
1	Opaque	Max 0.5 mm	Anhedral crystals and granular aggregates	Most near or within rock fragments
Trace	Hornblende(?)	Small, approximately euhedral crystals rimmed by opaque		

Percent Void Space: ~2% within matrix and as voids in pumice.

Welding: Dense to moderate. Similar to sample RMD-6, but pumice tends to retain somewhat more void space, although voids are strongly deformed by welding. Matrix shards are characteristically bent around competent crystals. Eutaxitic fabric is commonly very strong, but welding is not uniform throughout thin section.

Devitrification: Extensive, almost complete. Larger matrix shards show axiolitic structures, microlites showing birefringence are heavily dominant over isotropic areas, and even these areas may be cryptocrystalline. Matrix devitrification products include

- Reddish-brown iron oxide
- Low-relief clear crystals
- Pseudo-isotropic reddish to greenish materials

Devitrified pumice contains coarse, fan-shaped crystal aggregates, probably alkali feldspar and cristobalite(?), and small green (amphibole?) rods.

Miscellaneous Textures-Fabric: "Microgranitic" rock fragments appear to be devitrified volcanics or subvolcanics—crystals of quartz and alkali feldspar set in a matrix of radiating fan-shaped (feldspar-cristobalite?) aggregates, with lesser opaques and ferromagnesian minerals.

A rare rock fragment type contains reddish-brown spherulites.

Mesoscopic Description: Rock is a brick-red, densely welded ash-flow tuff characterized by extreme flattening of black obsidian-like pumice lenticles and bending of same around competent rock fragments. Degree of welding is approximately the same as in sample RMD-6.

Brick-red matrix is ~65% of rock; flattened black pumice lenticles, ~15%; crystals (dominantly alkali feldspar with subordinate quartz), ~3% to 4%. Remainder of mode is varicolored rock fragments (including white granodioritic types, perlitic gray fragments, and frothy brown material) and vapor-phase euhedral crystals filling small fractures and cavities.

Tuff Thin Section Description: Sample RMD-9

Petrographer: J. R. Connolly

Thin Section Orientation: Approximately perpendicular to eutaxitic foliation/layering

Location: Left rib of RMD, ~74 ft parallel to floor, 4 ft vertical

Rock Name: Moderately welded ash-flow tuff – Unit B

Constituents: (modes estimated visually; not representative because of large pumice fragment)

Modes Normalized to 100% Less Large Pumice	Est %	Fragment	Size-Range	Shape	Miscellaneous
50	39	Glass shards (~100% optically devitrified)	<1 mm	Strongly elongate	Axiolitic devitrification in larger shards
25	40 (half in one fragment)	Pumice	Few cm to <1 mm	Strongly flattened, commonly with irregular edges	Commonly highly devitrified; contains most porosity
13	10	Alkali feldspar	1 to 3 mm	Subhedral, commonly partly embayed, locally broken	Locally perthitic
5	4	Rock fragments	Up to 5 mm, avg 0.5 to 2 mm	Subrounded	Includes subvolcanics and fine-grained sediments
1	1	Quartz	<1 mm	Anhedral	Clear, uniform extinction
1	1	Opaque	<1 mm	Granular	Mostly blue-black rimming pyroxene or skeletal crystals in matrix
	Trace	Clinopyroxene	One crystal 3 x 10 mm plus smaller fragments	Euhedral to subhedral	Rimmed with opaques

Percent Void Space: Estimated ~5% in devitrified and nondevitrified pumice, and to a lesser extent in matrix and vugs.

Welding: Moderate. Pumice is largely devitrified, but bubbles are still present; bubbles are slightly flattened. Eutaxitic fabric is moderately well developed, and shards commonly are bowed-out around competent crystals.

Devitrification: Extensive. Large pumice is altered to coarse-grained, fan-shaped aggregates of alkali feldspar, quartz, or cristobalite, and pleochroic green to brown (amphibole?) rods. Matrix devitrification is also extensive, with three main products:

- Low-relief, low-birefringence, clear crystals
- Yellowish-brown, moderate relief, poorly crystalline, nonisotropic material
- Granular opaque

Miscellaneous Textures-Fabric: Glass shard texture appears to be largely obscured by devitrification. Outlines of relict glass shards are only visible in plane polarized light.

Mesoscopic Description: Brownish-gray, moderately welded ash-flow tuff. Rock is 70% to 75% gray matrix, 8% to 10% crystals (chiefly sanidine ± quartz), and occasional granitic lithic fragments. Vapor-phase minerals are present in vesicles of pumice fragments, rimming pumice lenticles, and in vugs and small fractures. Frothy brown fragments may represent vapor-phase filling or uncollapsed pumice. Degree of flattening of lenticles is less and, although pumice is dark in color, porosity is still present.

This sample is adjacent to Drill Hole RMD-11, core hole to be tested for porosity and strength by Sandia.

Tuff Thin Section Description: Sample RMD-10

Petrographer: J. R. Connolly

Thin Section Orientation: Approximately perpendicular to layering

Location: Left rib of RMD, ~88.5 ft parallel to floor, 2.5 ft vertical

Rock Name: Slightly welded ash-flow tuff – Unit C

Constituents: (modes estimated by 385 point count)

Est %	Fragment	Size-Range	Shape	Miscellaneous
56 (43% devitrified, 13% isotropic)	Glass shards	Recognizable shards <0.5 mm	Weakly elongate, parallel to layering	Shard structure only locally preserved because of devitrification
6*	Pumice	Several millimetres to <1 mm	Variable: crescent shape to subrounded	Extensively devitrified
14*	Coarse, devitrified products	<0.3 mm in large aggregate areas	Individual crystals; shape highly variable	
11	Alkali feldspar	<0.5 mm to 4 mm	Subhedral, commonly broken	Probably anorthoclase
3*	Rock fragments	Between 1 and 3 mm	Rounded to subrounded	Fine-grained cherty argillite dominant, subordinate volcanics
2	Opaque	Highly variable, patches to granules, brown, probably hydrated Fe oxides		
2	Quartz	<1 mm	Anhedral to subhedral, broken	
Trace	Altered microcline, Altered pyroxene, or Olivine			

*Modal proportions of rock fragments and pumice may be higher because of inclusion in coarse-grained devitrification products.

Percent void space: ~6%; includes void space in matrix and pumice.

Welding: Slight. Pumice is undeformed to only slightly collapsed, and original voids are largely preserved without obvious distortion. Glass shards are not common, possibly as a result of extensive devitrification and alteration. Where shard structures can be recognized, there is no obvious or strong preferred orientation.

Devitrification: Extensive, almost complete. Coarse devitrification products include vug-filling, vapor-phase crystals, and aggregate mosaics of crystals replacing pumice and rock fragments, and filling fracture-like zones. Three main crystal types are

- Needle-shaped brown amphiboles(?)
- Radiating crystal aggregates with low-relief (alkali feldspar and quartz?)
- Brownish-yellow granules with moderate relief

Shards are almost completely altered to a mix of low-birefringence, small, clear crystals, yellowish high-relief granules, and dark, high-relief isotropic to opaque minerals. The difference in morphology of matrix crystallization suggests that much may have occurred at low temperature after devitrification and welding.

Miscellaneous Textures-Fabric: Crystallization products partly or completely filling vugs are common, although unfilled matrix porosity is present.

Mesoscopic Description: Rock is dark brown, slightly to moderately welded with only moderate deformation of light brown, devitrified pumice fragments. Rock is rich in crystals (~20%, chiefly alkali feldspar and minor biotite(?)) and vapor-phase minerals, with vugs as large as 5 cm partly to completely filled. Overall, rock has a very dirty, altered appearance.

Tuff Thin Section Description: Sample RMD-11

Petrographer: J. R. Connolly

Thin Section Orientation: Approximately perpendicular to layering

Location: Working face of RM Alcove (11/7/80); from reddish-brown Transition Zone above the Grouse Canyon Member

Rock Name: Moderately welded ash-flow tuff

Constituents: (modes estimated by visual inspection)

Est %	Fragment	Size-Range	Shape	Miscellaneous
70	Glass shards	0.5 mm or less	Elongate, rare Y & V shapes	Strong preferred orientation
2	Pumice	Generally <1 mm	Subrounded to flattened	Mostly collapsed types, some porosity present
8	Alkali feldspar	Max 2 mm, avg <1 mm	Subhedral, broken	Estimate includes a few plagioclase crystals
2	Quartz	<0.5 mm	Commonly anhedral, broken	Locally embayed, resorbed
3	Rock fragments	Generally <1 mm	Subrounded to subangular	Most tuffaceous volcanic with cherty to argillaceous sediments, rare metamorphics
1	Opaque	<0.5 mm	Granular, subhedral	
Trace	Pyroxene, olivine	<1 mm	Subhedral to anhedral, most rounded, altered	
Trace	Vapor-phase minerals	Crystal aggregates, in cavities, may include some zeolites		

Percent void space: ~15%; may be less. Difficult to estimate because of plucking.

Welding: Probably moderate as suggested by strong preferred orientation of shards. Rock shows fairly good sorting of nonshard fragments and may represent the distal portion of an overlying ash-flow not related to the underlying Grouse Canyon Member.

Devitrification: Appears moderate, but may be more extensive. Glass shards show small-scale microlite development and, rarely, a weak axiolitic structure. Shards are brown in plane polarized light and appear to be microcrystalline when viewed at high magnification. Reddish-brown color is suggestive of some oxidation.

Miscellaneous Textures-Fabric: Average grain size 0.5 to 1 mm; sorting good—crystals are larger than shards, but all nonshard fragments are of generally uniform size. Porosity is only partly filled by vapor-phase minerals and authigenic zeolites(?).

Presence of resorbed quartz, plagioclase, pyroxene, olivine, and a different mix of rock fragments suggests that this unit may be genetically unrelated to the underlying Grouse Canyon Member.

Mesoscopic Description: Rock is medium reddish-brown, composed of fine, sand-size grains with sparse, small (1/2 to 1 mm) crystals of alkali feldspar common. Good sorting suggests possible origin in distal portion of ash flow or secondary sedimentary transport and deposition.

Table B2. Sample Descriptions (Mesoscopic) of Fracture Filling and Clay Samples

RMD-3:	Left rib of RMD, 17.5 ft horizontal from beginning of drift, 2.5 ft vertical from floor. Sample is mostly of matrix clay, reddish-brown in color, forming the primary cementing agent for 5.5-ft-thick depositional "rubble zone" (or volcanic breccia). Clasts (not sampled except for small fragments included in the clay) are mostly dark reddish-brown to brown ash-flow tuff with subordinate nonvolcanic constituents including granitic(?) and argillitic clasts.
RMD-5:	Left rib of RMD, 40.5 ft horizontal from beginning of drift, 5.7 ft vertical, adjacent to curved fracture. Occurs as ovoid, approximately baseball-sized (~8 cm) pod of greenish clay with subordinate reddish-brown lithic material. May be devitrified and subsequently argillitized pumice fragment.
RMD-8:	Left rib of RMD, 64 ft horizontal from beginning of drift, 1 ft vertical from floor. Densely welded reddish-brown ash-flow tuff essentially identical to sample RMD-7. This sample contains slickensides as a highly polished, very thin surface ring. Slickensides here are subhorizontal and approximately parallel with the bearing of the drift (N 35°W).
RMD-12:	From left rib of Rock Mechanics Alcove (RMA), ~3 ft from RMD, 8 ft vertical from floor. Occurs as an ~1-cm-thick, 10+ cm-long seam parallel to layering in poorly welded upper part of Grouse Canyon Member ~6 ft below base of the Transition Zone. Material is a mixture of greenish-yellow and dark greenish-gray clay occurring as a discrete pod within dark brown, altered-appearing, poorly welded tuff.
RMD-13:	From left rib of RMA, ~5 ft from RMD, 6 ft vertical from floor. Occurs as small pod, ~3 x 2 cm within the poorly welded upper part of the Grouse Canyon Member. Pod has core of white (bleached?) material surrounded by halo of reddish-brown oxidized material. May represent a completely altered rock or pumice fragment.
RMD-14:	From working face of RMA (as of 11/7/80), ~4 ft up from floor, ~2 ft from left rib. Reddish-brown clay pod, appears to be altered pumice or rock fragment ~5 cm diameter. Pod is surrounded by a rim of pale buff material (not sampled).
RMD-15:	From working face of RMA (as of 11/7/80), ~4 ft up from floor, 5.5 ft from left rib. Occurs as elongate pod flattened in layering and extended perpendicular to the face (which strikes N 35°W)—dimensions are ~1.5 x 5 x 10 cm. Material is dark yellowish-green clay with local splotchy appearance, suggesting possible presence of several clay minerals. Host rock is poorly welded upper part of Grouse Canyon Member ~6 ft below base of Transition Zone.
RMD-16:	Right rib of RMA, 3.5 ft in from RMD, ~5.5 ft below base of Transition Zone. Sample is from a dark brownish-buff, clay-rich seam ~2 cm wide within a subvertical tectonic breccia zone striking ~N 80°W. Sample is dark-brown clay with a lighter brown-to-buff, silty fraction.
LA-1 & LA-2:	Samples taken in Laser Alcove adjacent to heater test pad. LA-1 is from center of fault-fracture filling clay seam, LA-2 is from rim. Seam is ~10 cm (4 in.) wide with subhorizontal slickensides on edge. Clay seam is enclosed in breccia. LA-1: light brownish-buff clay making up most of seam. LA-2: thin rind (avg 0.5 cm) of brick-red clay, locally slickensided with black coating on edge of seam. This zone is similar to the one from which RMD-16 was taken, except that this seam is much wider.

Table B3. Petrographic Observations of Supplemental Sample U12G RM-P1-30.0*

Thirty-foot depth in core hole RM-P1. From lower Rubble Flow Zone. Matrix here is hard and well-indurated rock in contrast to soft clayey material in RMD-3 sample. Matrix is devitrified shards in which much of matrix is microcrystalline, and shards are commonly not recognizable as such. Approximately 25% of mode is yellowish-brown shards that show axiolitic devitrification. Vesicles are common, average 0.5 mm across, and are lined with vapor-phase minerals (quartz or tridymite + alkali feldspar). Welding is slight, and preferred orientation of constituent shards and clasts is weak. Crystal fragments and rock fragments are commonly subangular to subrounded. The Rubble Flow Zone probably originated as a hot volcanic breccia or base surge-type deposit within the compound cooling unit of the Grouse Canyon Member. The extensive alteration of this matrix to reddish-brown clay in the Rock Mechanics Drift (Sample RMD-3) is probably caused by later, local alteration by groundwater that did not affect the sample from the core hole.

*Petrographer: J. R. Connolly

APPENDIX C

Detailed X-Ray Results for Individual Samples

Sample RMD-3

<2 μm fraction

degrees 2θ						
untreated	5	6-9	19.6	22-22.5	26.8	27.6
glycolated			5.4			

The sharp peak at about 5° and 19.6° is a smectite, probably saponite.

The broad peak at 6° to 9° is probably a poorly crystallized, mixed-layer illite/smectite.

Peaks at 22.4° and 27.6° are feldspar. 26.8° is quartz.

Upon glycolation, the saponite and illite/smectite structures expand. The broad peak at 5.4° on the glycolated sample is illite/smectite. The expansion of saponite is probably represented by a small peak at 4.3°.

No zeolites were identified.

>2 μm, <100 mesh

Poorly crystallized illite/smectite is dominant; quartz and feldspar are present.

Sample RMD-5

<2 μm fraction

degrees 2θ		
untreated	6	18
glycolated	5.4	

The sample is smectite or Fe-rich swelling chlorite. The 18° peak is typically the (003) reflection of chlorite.

>2 μm, <100 mesh

The clay mineral identified in the finer fraction is dominant.

Sample RMD-12

<2 μm fraction

degrees 2θ		
untreated	5.05	6.1
glycolated		5.1

The sample contains the 5° peak of saponite. The 6.1° peak (14.4 Å) is characteristic of chlorite. The expansion of the chlorite structure upon glycolation is indicative of a swelling chlorite. These are the only two minerals present.

<2 μm, <100 mesh

Clay minerals identified in the fine fraction are dominant.

Sample RMD-13

White material:

Whole-rock fraction

degrees 2θ					
4.8	7	15	20	26.8	28

The very broad peaks at 7°, 15°, and 20° indicate a poorly crystalline smectite. 26.8° is quartz, and 28° is probably feldspar.

Red material:

Whole-rock fraction

degrees 2θ		
5.4	7	20

The 5.4° peak is saponite, and the 7° and 20° peaks represent other smectite varieties.

Sample RMD-14

<2 μm fraction

degrees 2θ						
untreated	5.4	8.8	23.6	25.8	26.8	27.6
glycolated	5.4					

Saponite (5.4°) is dominant, with minor amount of mixed-layer illite/smectite (8.8°). 23.6°, 25.8°, and 27.6° are feldspar peaks; 28.8° is quartz.

>2 μm, <100 mesh

Saponite is dominant.

Sample RMD-15

<2 μm fraction

degrees 2θ				
untreated	6.2		18	20
glycolated	5.4	10.8		

The 6.2° and 18° peaks are chlorite or a mixed-layer chlorite/smectite.

Sample RMD-16

<2 μm fraction

degrees 2θ				
untreated	5.1	6	26.8	27.8
glycolated	5.4			

The 5.1° peak is saponite, and the dominant clay mineral (6°) is a different smectite. 26.8° is quartz; 27.8° is feldspar. The smectite expands upon glycolation.

>2 μm, <100 mesh

degrees 2θ					
5.2	10	22.6	22.8	26.8	27.8

Clay minerals are dominant (5.2°), with subordinate quartz (26.8°) and feldspar (27.8°). Minor clinoptilolite (10°, 22.6°, 22.8°) is present.

Sample LA-1

<2 μm fraction

degrees 2θ		
untreated	5.2	6
glycolated	5.3	

Saponite (5.2°) is subordinate to swelling smectite (6°).

>2 μm, <100 mesh

Some clay minerals present as in fine fractions. No zeolites identified.

Sample LA-2

<2 μm

degrees 2θ		
untreated	5-6 (broad)	27.6
glycolated	5.2	

Poorly crystalline saponite and smectite are dominant; 27.6° is feldspar.

DISTRIBUTION:

TIC-4500-R70, UC-70 (310)

US Department of Energy, NE-22 (6)
Office of Waste Isolation
Germantown, MD 20767
Attn: W. W. Ballard, Jr., Director
R. Stein, Team Leader
C. R. Cooley, Team Leader
C. H. George, Team Leader
J. J. Fiore
J. W. Bennett

US Department of Energy, NE-20
Office of Terminal Waste Disposal
& Remedial Action Nuclear Energy
Germantown, MD 20767
Attn: F. E. Coffman, Acting Director

US Department of Energy
Projects & Facilities Management
Richland Operations Office
Richland, WA 99352
Attn: J. H. Anttonen, Assistant Manager

US Nuclear Regulatory Commission (3)
Division of Waste Management
High-Level Waste Technical
Development Branch
Washington, DC 20555
Attn: NTS Project Manager (2)
Chief, High-Level Waste Technical
Development Branch

US Department of Energy
National Waste Terminal
Storage Program Office
505 King Avenue
Columbus, OH 43201
Attn: J. O. Neff, Program Manager

Battelle (7)
Office of Nuclear Waste Isolation
505 King Avenue
Columbus, OH 43201
Attn: N. E. Carter
S. Goldsmith
ONWI Library (5)

Battelle
Office of NWTS Integration
505 King Avenue
Columbus, OH 43201
Attn: W. A. Carbiener

Los Alamos National Laboratory (2)
PO Box 1663
Los Alamos, NM 87545
Attn: D. T. Oakley, Tech Project Officer, MS F-671
D. C. Hoffman, MS 760

Rockwell International Atomics
International Division
Rockwell Hanford Operations
Richland, WA 99352
Attn: R. Deju

Governor's Office of Planning
Coordination
State of Nevada
Capitol Complex
Carson City, NV 89023
Attn: R. M. Hill, State Planning Coord

Department of Energy
State of Nevada
Capitol Complex
Carson City, NV 89710
Attn: S. A. Robinson

Lawrence Livermore National Laboratory
PO Box 808, MS L-209
Livermore, CA 94550
Attn: K. Street, Jr.

Lawrence Livermore National Laboratory
PO Box 808, MS L-204
Livermore, CA 94550
Attn: L. D. Ramspott, Tech Project Officer

US Geological Survey
PO Box 25046, MS 416
Federal Center
Denver, CO 80225
Attn: W. W. Dudley, Jr.,
Tech Project Officer

W. S. Twenhofel
820 Estes Street
Lakewood, CO 80215

US Department of Energy (5)
Waste Management Project Office
PO Box 14100
Las Vegas, NV 89114
Attn: D. L. Vieth, Director

DISTRIBUTION (Cont):

US Department of Energy
Office of Public Affairs
PO Box 14100
Las Vegas, NV 89114
Attn: D. F. Miller, Director

US Department of Energy (8)
PO Box 14100
Las Vegas, NV 89114
Attn: D. A. Nowack

US Department of Energy
Health Physics Division
PO Box 14100
Las Vegas, NV 89114
Attn: B. W. Church, Director

Holmes & Narver, Inc.
PO Box 14340
Las Vegas, NV 89114
Attn: A. E. Gurrola

Reynolds Electrical & Engineering
Company, Inc.
PO Box 1440, MS 555
Las Vegas, NV 89114
Attn: H. D. Cunningham

Fenix & Scisson, Inc.
PO Box 15408
Las Vegas, NV 89114
Attn: J. A. Cross

US Department of Energy
CP-1, M/S 210
PO Box 14100
Las Vegas, NV 89114
Attn: R. H. Marks

Westinghouse – AESD
PO Box 708, MS 703
Mercury, NV 89023
Attn: A. R. Hakl, Site Manager

Lawrence Livermore National Laboratory
PO Box 808, MS L-204
Livermore, CA 94550
Attn: A. J. Rothman

US Department of Energy (2)
Technical Information Center
PO Box 62
Oak Ridge, TN 37830

7254 F. W. Muller
9700 E. H. Beckner
9731 A. R. Lappin (30)
9760 R. W. Lynch
9761 L. W. Scully
9762 J. K. Johnstone
9762 B. S. Langkopf
9762 F. B. Nimick
9762 L. D. Tyler
9763 J. R. Tillerson
9763 R. M. Zimmerman
9764 A. E. Stephenson
8214 M. A. Pound
3141 L. J. Erickson (5)
3151 W. L. Garner (3)

☆U.S. GOVERNMENT PRINTING OFFICE: 1983-0-676-027/554